NATIONAL AERONAUTICS AND SPACE ADMINISTRATION

Technical Report 32-1471

Minimum Energy Control of a Class of Electrically Driven Vehicles

Y. E. Sahinkaya

JET PROPULSION LABORATORY
CALIFORNIA INSTITUTE OF TECHNOLOGY
PASADENA, CALIFORNIA

May 1, 1970

NATIONAL AERONAUTICS AND SPACE ADMINISTRATION

Technical Report 32-1471

Minimum Energy Control of a Class of Electrically Driven Vehicles

Y. E. Sahinkaya

JET PROPULSION LABORATORY
CALIFORNIA INSTITUTE OF TECHNOLOGY
PASADENA, CALIFORNIA

May 1, 1970

Prepared Under Contract No. NAS 7-100
National Aeronautics and Space Administration

Preface

The work described in this report was performed by the Guidance and Control Division of the Jet Propulsion Laboratory.

Acknowledgment

The author wishes to express his gratitude to Mr. H. K. Bouvier for his support during the mechanization of the minimum energy control law. Appreciation is also extended to Mr. A. Baca for his assistance during the laboratory work. The theoretical results of this investigation were obtained during graduate studies at the California Institute of Technology, under the supervision of Prof. R. Sridhar.

Contents

Figures

Contents (contd)

Figures (contd)

Abstract

An automatic speed controller has been designed and built for a class of electrically driven vehicles according to the theoretical concepts determined by the application of modern control theory. The theoretical and practical results given in this report are originally aimed at the design and development of an automatic speed controller for lunar-roving vehicles. For the vehicle considered, each wheel is driven by a permanent-magnet dc motor whose speed is governed by a controller with the following operational characteristics:

(1) The controller accelerates or decelerates the vehicle to the desired speed in response to a command signal fed into the system by the throttle mechanism in the presence of vehicle disturbances caused by terrain slope changes.

(2) The controller maintains a constant vehicle speed at the desired value in the presence of terrain slope changes.

(3) The controller accomplishes the above by using a minimum amount of battery energy for the motor armature circuit during acceleration, and by feeding a maximum amount of energy from the motor armature circuit to the battery during deceleration.

A single wheel automatic speed controller, with the salient features specified has been built and successfully tested in the laboratory. The test results are also applicable to many other electric drive systems with different power ratings using permanent-magnet, or separately excited dc motors.

Minimum Energy Control of a Class of Electrically Driven Vehicles

I. Introduction

In recent years, following the pioneering works of Pontryagin, Bellman, and Kalman, an intense amount of research has been carried out by many workers in the area of modern control theory. The optimization techniques of modern control theory along with digital computers provide a new approach for the design of automatic control systems.

One of the most challenging tasks in the formulation of a practical problem in the context of optimal control theory is the selection of an appropriate performance index. Even though an adequate mathematical description of the plant is available, the quality of the result obtained by the application of optimal control theory is dependent upon the selection of a meaningful performance index.

This report briefly discusses the theoretical work that was carried out during the formulation and solution of minimum-energy control problems associated with a class of electrically driven vehicles in the context of modern control theory. Also, the report describes in detail the concepts used during the design and the mechanization of the resulting control law in the light of current engineering practice.

II. Theoretical Results

A. Formulation

The plant, or process to be controlled (Ref. 1), is described by the following ordinary linear differential equations:

$$\dot{x}_1(t) = -\left(\frac{f}{J} + \frac{k_t k_b}{Jr}\right) x_1(t) - \left(\frac{f}{J} + \frac{k_t k_b}{Jr}\right) \alpha - \left(\frac{1}{J}\right) x_2(t) - \left(\frac{1}{J}\right) x_3(t) + \left(\frac{k_t}{Jr}\right) u(t) \tag{1}$$

$$\dot{x}_2(t) = -(\omega_0) x_2(t) + \xi_w(t) \tag{2}$$

$$\dot{x}_3(t) = 0 \tag{3}$$

where

$x_1(t) \triangleq x(t) - \alpha$

$x(t) \triangleq$ angular speed of electric motor; linearly proportional to speed of vehicle, rad/s

$\alpha \triangleq$ desired speed of electric motor, rad/s

$\xi_w(t) \triangleq$ stationary Gaussian, white-noise process having zero mean and spectral density $2\omega_0\sigma_c^2$, Nm/s

$x_2(t) \triangleq$ stationary Gaussian, exponentially correlated-noise process having zero mean, variance σ_c^2, and correlation time $(1/\omega_0)$, Nm

$x_3(t) \triangleq$ constant but arbitrary disturbance torque, Nm. The sum of $x_2(t)$ and $x_3(t)$ represents a stochastic process that describes the effects of terrain slope changes on the dynamical behavior of the system. If $x_2(t) \equiv 0$ in $0 \leq t \leq T$, the vehicle is said to be moving on a terrain with a constant slope angle

$u(t) \triangleq$ control voltage, V. Control voltage is applied to the armature circuit of a permanent-magnet dc motor

$J \triangleq$ total system inertia as referred to motor, Nm/rad/s.^{2} The total system inertia, represented by J, is the effective inertia of the system at the motor shaft, and is a known function of the inertias of the motor rotor, wheel and tire assembly, and total mass of the vehicle.

$f \triangleq$ total system damping coefficient as referred to motor, Nm/rad/s. The total system damping coefficient, represented by f, is the effective damping coefficient of the system at the motor shaft, and is a known function of the viscous friction in the motor, wheel bearings, and velocity-dependent component of the rolling friction between the terrain surface and the tires of the vehicle

$k_t \triangleq$ motor torque constant, Nm/A

$k_b \triangleq$ motor back-emf constant, V/rad/s

$r \triangleq$ motor resistance, Ω

In the derivation of Eq. (1) the following assumptions have been made:

(1) The electric motor propulsion force is transmitted to the vehicle wheel through a speed-reducer without slippage between the tires and the terrain surface. Each wheel of the vehicle is driven by a permanent-magnet dc motor and total vehicle load is shared equally by the wheels.

(2) The aerodynamic drag force is negligible because of low-speed operation.

(3) The mechanical system parameters (J,f) and armature resistance r are constants.

(4) The motor armature inductance is negligible.

(5) The motor operation is unsaturated.

The performance index for this optimization problem is selected to be the electric energy consumption of the system and is given by:

$$E = F_w x_1^2(T) + \int_0^T \left\{ \frac{u^2(t) - k_b u(t)\,[x_1(t) + \alpha]}{r} \right\} dt \tag{4}$$

where

$T \triangleq$ response time which is fixed but arbitrary

$F_w \triangleq$ weighting factor

The weighting factor F_w is artificially introduced to facilitate the use of Bellman's dynamic programming technique. The integrand in Eq. (4) represents the electric power that can flow from a rechargeable battery system into the motor circuit or from the motor circuit into the battery over different intervals of time during the controlling process.

The set of boundary conditions to be satisfied by the state variables for three cases of control action are as follows:

(1) Case 1, speed-control:

$$\left.\begin{aligned} x_1(0) &= 0, & x_1(T) &= 0 \\ x_2(0) &= 0, & x_2(T) &= \text{free} \\ x_3(0-) \neq x_3(0) &= \beta, & x_3(T) &= \beta \end{aligned}\right\} \tag{5}$$

(2) Case 2, speed-setting:

$$\left.\begin{aligned} x_1(0) &= x(0) - \alpha, & x_1(T) &= 0 \\ x_2(0) &= 0, & x_2(T) &= \text{free} \\ x_3(0-) &= x_3(0) = \beta, & x_3(T) &= \beta \end{aligned}\right\} \tag{6}$$

(3) Case 3, speed-control and speed-setting:

$$\left.\begin{aligned} x_1(0) &= x(0) - \alpha, & x_1(T) &= 0 \\ x_2(0) &= 0, & x_2(T) &= \text{free} \\ x_3(0-) &\neq x_3(0) = \beta, & x_3(T) &= \beta \end{aligned}\right\} \tag{7}$$

The statement of the control problem is as follows: given the linear time-invariant system [Eqs. (1), (2), and (3)], the performance index [Eq. (4)], an arbitrary response time T, and unconstrained $u(t)$, determine $u(t)$ to satisfy the boundary conditions on $x_1(t)$ [as described by Eq. (5) for speed-control, Eq. (6) for speed-setting, and Eq. (7) for speed-control and speed-setting] and to minimize the performance index.

In reality, the control voltage $u(t)$ is constrained by the inequality

$$0 \leq u(t) \leq U \tag{8}$$

where U = battery voltage.

The battery voltage U is assumed to be constant in $0 \leq t \leq T$. In this particular optimization problem, U will be determined as part of the solution. It is extremely important to note that if the integrand in Eq. (4) is positive over a finite interval of time in $0 \leq t \leq T$, then the electrical energy supplied by the battery is used to satisfy mechanical energy requirements of the system, and electrical and mechanical energy losses are minimized by the optimal choice of $u(t)$. During this time, armature current for the motor is supplied from the battery. If the integrand in Eq. (4) is negative over a finite interval of time in $0 \leq t \leq T$, then the mechanical energy available in the system is used to satisfy mechanical energy requirements of the system while yielding a maximum amount of electrical energy that can be used to charge the battery. This is accomplished by the optimal choice of $u(t)$ to minimize the total electrical and mechanical energy losses over that particular interval of time. During this time, the armature current of the motor flows from the motor armature to the battery.

B. Solution

The solution of this stochastic optimization problem is obtained as follows. Define the optimal expected value function for this optimization by

$$S(t,\mathbf{x}) = \min_{u(t)} \epsilon_{\xi_w(t)} \times \left(F_w x_1^2(T) + \int_t^T \left\{ \frac{u^2(\tau) - k_b u(\tau)[x_1(\tau) + \alpha]}{r} \right\} d_\tau \right) \tag{9}$$

where $\epsilon[\cdot] \triangleq$ expectation operator.

Applying the standard procedure (see Ref. 1) to Eq. (9) yields

$$u^*(t) = \left(\frac{k_b}{2}\right)[x_1(t) + \alpha] - \left(\frac{k_t}{2J}\right) S_{x_1}(t,\mathbf{x}) \tag{10}$$

where

$$\mathbf{x} \triangleq \text{state vector}$$

$$S_{x_1}(t,\mathbf{x}) = \frac{\partial}{\partial x_1} S(t,\mathbf{x})$$

and $S_{x_1}(t,\mathbf{x})$ is obtained by solving the following Bellman–Hamilton–Jacobi equation:

$$\begin{aligned} S_t(t,\mathbf{x}) &- \left(\frac{c}{2}\right)[x_1(t) + \alpha]^2 - a[x_1(t) + \alpha] S_{x_1}(t,\mathbf{x}) \\ &- \left(\frac{b}{2}\right) S_{x_1}^2(t,\mathbf{x}) - \left(\frac{1}{J}\right) x_2(t) S_{x_1}(t,\mathbf{x}) \\ &- \left(\frac{1}{J}\right) x_3(t) S_{x_1}(t,\mathbf{x}) - (\omega_0) x_2(t) S_{x_2}(t,\mathbf{x}) \\ &+ (\omega_0 \sigma_c^2) S_{x_2 x_2}(t,\mathbf{x}) = 0 \end{aligned} \tag{11}$$

with the boundary condition

$$S(T,\mathbf{x}) = F_w x_1^2(T) \tag{12}$$

where

$$a = \left(\frac{f}{J} + \frac{k_t k_b}{2Jr}\right), \qquad a > 0$$

$$b = \left(\frac{k_t^2}{2J^2 r}\right), \qquad b > 0$$

$$c = \left(\frac{k_b^2}{2r}\right), \qquad c > 0$$

$$S_t(t,\mathbf{x}) = \frac{\partial}{\partial t} S(t,\mathbf{x})$$

$$S_{x_2}(t,\mathbf{x}) = \frac{\partial}{\partial_{x_2}} S(t,\mathbf{x})$$

$$S_{x_2x_2}(t,\mathbf{x}) = \frac{\partial^2}{\partial x_2 \partial x_2} S(t,\mathbf{x})$$

Let

$$S(t,\mathbf{x}) = \tfrac{1}{2} <\mathbf{x},\mathbf{P}(t)\,\mathbf{x}> + \mathbf{q}\,\mathbf{x} + h(t) \tag{13}$$

where

$\mathbf{P}(t) \triangleq 3 \times 3$ symmetric matrix

$<,> \triangleq$ inner product of two vectors

$\mathbf{q} \triangleq$ raw vector with three components

$h(t) \triangleq$ a scalar function

Determining $S_t(t,\mathbf{x})$, $S_{x_1}(t,\mathbf{x})$, $S_{x_2}(t,\mathbf{x})$, and $S_{x_2x_2}(t,\mathbf{x})$ from Eq. (13), substituting these into Eq. (11), collecting the coefficients of equal powers of x, and equating them to zero, yields the following equations:

$$\dot{P}_{11}(t) - bP_{11}^2(t) - 2aP_{11}(t) - c = 0 \tag{14}$$

$$P_{11}(T) = 2F_w \tag{15}$$

$$\dot{P}_{12}(t) - [a + bP_{11}(t) + \omega_0]P_{12}(t) - \left(\frac{1}{J}\right) P_{11}(t) = 0 \tag{16}$$

$$P_{12}(T) = 0 \tag{17}$$

$$\dot{P}_{13}(t) - [a + bP_{11}(t)]P_{13}(t) - \left(\frac{1}{J}\right) P_{11}(t) = 0 \tag{18}$$

$$P_{13}(T) = 0 \tag{19}$$

$$\dot{P}_{22}(t) - (2\omega_0)P_{22}(t) - bP_{12}^2(t) - \left(\frac{2}{J}\right)P_{12}(t) = 0 \tag{20}$$

$$P_{22}(T) = 0 \tag{21}$$

$$\dot{P}_{23}(t) - \omega_0 P_{23}(t) - bP_{12}(t)P_{13}(t) - \left(\frac{1}{J}\right)[P_{12}(t) + P_{13}(t)] = 0 \tag{22}$$

$$P_{23}(T) = 0 \tag{23}$$

$$\dot{P}_{33}(t) - bP_{13}^2(t) - \left(\frac{2}{J}\right) P_{13}(t) = 0 \tag{24}$$

$$P_{13}(T) = 0 \tag{25}$$

$$\dot{q}_1(t) - [a + bP_{11}(t)]q_1(t) - (a\alpha)P_{11}(t) - \alpha c = 0 \tag{26}$$

$$q_1(T) = 0 \tag{27}$$

$$\dot{q}_2(t) - \omega_0 q_2(t) - \left[\frac{1}{J} + bP_{12}(t)\right] q_1(t) - (a\alpha)P_{12}(t) = 0 \tag{28}$$

$$q_2(T) = 0 \tag{29}$$

$$\dot{q}_3(t) - a\alpha P_{13}(t) - bP_{13}(t)q_1(t) - \left(\frac{1}{J}\right) q_1(t) = 0 \tag{30}$$

$$q_3(T) = 0 \tag{31}$$

$$\dot{h}(t) - \left(\frac{b}{2}\right) q_1^2(t) - (a\alpha)q_1(t) - \left(\frac{c}{2}\right)\alpha^2 + (\omega_0\sigma_c^2)P_{22}(t) = 0 \tag{32}$$

$$h(T) = 0 \tag{33}$$

From Eq. (13) an equation can be obtained for $S_{x_1}(t,\mathbf{x})$, and the terms $P_{11}(t)$, $P_{12}(t)$, $P_{13}(t)$, and $q_1(t)$ can be determined by analytically solving Eqs. (14), (16), (18), and (26) using their corresponding boundary conditions. The results are

$$P_{11}(t) = -\left(\frac{a}{b} - \left[\frac{(d)^{1/2}}{b}\right]\left\{\frac{\cosh[(d)^{1/2}(T-t)]}{\sinh[(d)^{1/2}(T-t)]}\right\}\right) \tag{34}$$

$$P_{12}(t) = \left[\frac{1}{Jb(\omega_0^2 - d)}\right]\left(a\omega_0 + d + (d)^{1/2}(a + \omega_0)\left\{\frac{\exp[-\omega_0(T-t)] - \cosh[(d)^{1/2}(T-t)]}{\sinh[(d)^{1/2}(T-t)]}\right\}\right) \tag{35}$$

Note that as $\omega_0^2 \to d$, $\lim P_{12}(t)$ exists.

$$P_{13}(t) = -\left\{\frac{1}{Jb\sinh[(d)^{1/2}(T-t)]}\right\}\left(\sinh[(d)^{1/2}(T-t)] - \frac{a}{(d)^{1/2}}\{\cosh[(d)^{1/2}(T-t)] - 1\}\right) \tag{36}$$

$$q_1(t) = \left\{\frac{-\alpha(d)^{1/2}}{b\sinh[(d)^{1/2}(T-t)]}\right\}\left(\frac{a}{(d)^{1/2}}\sinh[(d)^{1/2}(T-t)] - \cosh[(d)^{1/2}(T-t)] + 1\right) \tag{37}$$

where $d \triangleq a^2 - bc$ and operation $\lim F_w \to \infty$ has been performed on the expressions obtained from solution of Eqs. (14), (16), (18), and (26). This operation guarantees that as $t \to T$, $\lim x_1(t) = 0$.

Hence, the following control law is obtained:

$$\begin{aligned} u^*(t) = {} & \left(\frac{k_b}{2} + \frac{k_t a}{2Jb} + \left\{\frac{1-\cosh[(d)^{1/2}(T-t)]}{\sinh[(d)^{1/2}(T-t)]}\right\}\left[\frac{k_t(d)^{1/2}}{2Jb}\right]\right)x(t) \\ & + \left(\frac{k_t}{2J^2b} + \left\{\frac{1-\cosh[(d)^{1/2}(T-t)]}{\sinh[(d)^{1/2}(T-t)]}\right\}\left[\frac{k_t a}{2J^2b(d)^{1/2}}\right]\right)x_3(t) + \left\{\left(\frac{1}{\sinh[(d)^{1/2}(T-t)]}\right)\left[\frac{k_t(d)^{1/2}}{2Jb}\right]\right\}[\alpha - x(t)] \\ & - \left(a\omega_0 + d + \left\{\frac{\exp[-\omega_0(T-t)] - \cosh[(d)^{1/2}(T-t)]}{\sinh[(d)^{1/2}(T-t)]}\right\}[(d)^{1/2}(a+\omega_0)]\right)\left[\frac{k_t}{2J^2b(\omega_0^2 - d)}\right]x^2(t) \end{aligned} \tag{38}$$

In Eq. (38), making the following approximations:

$$\left\{\frac{1-\cosh[(d)^{1/2}(T-t)]}{\sinh[(d)^{1/2}(T-t)]}\right\} \equiv \lim_{t\to T}[\cdot] = 0$$

$$\left(a\omega_0 + d + (d)^{1/2}(a+\omega_0)\left\{\frac{\exp[-\omega_0(T-t)] - \cosh[(d)^{1/2}(T-t)]}{\sinh[(d)^{1/2}(T-t)]}\right\}\right) \equiv \lim_{t\to T}[\cdot] = -(\omega_0^2 - d)$$

yields the following suboptimal solution for the stochastic control problem:

$$u_{so}(t) = \left(k_b + \frac{rf}{k_t}\right)x(t) + \left(\frac{r}{k_t}\right)v(t) + \left[\frac{fr}{k_t}\left(1 + \frac{k_t k_b}{fr}\right)^{1/2}\right]\left\{\frac{1}{\sinh\left[\frac{f}{J}\left(1 + \frac{k_t k_b}{fr}\right)^{1/2}(T-t)\right]}\right\} \cdot [\alpha - x(t)] \tag{39}$$

where

$$v(t) \triangleq x_2(t) + x_3(t) \tag{40}$$

The result given by Eq. (39) is important in that it is much easier in practice to measure the disturbance torque $v(t)$, which is the sum of state variables $x_2(t)$ and $x_3(t)$, rather than to measure each variable separately. Hence, the implementation of the control law given by Eq. (39) is straightforward. The implementation of the control law given by Eq. (38) cannot be accomplished unless a Kalman filter is used to estimate the state vector $\mathbf{x}$ from the measurable states. This follows from the concept of the separation principle that allows the estimation of the state vector $\mathbf{x}$ and the computation of the control law to be performed independently (see Ref. 1).

Some interesting features of the solution for this optimization problem are obtained as follows:

Let

$$x(t) = x_d(t) + \tilde{x}(t) \tag{41}$$

where

$$x_d(t) \triangleq \epsilon[x(t)]$$

$$x(t) \triangleq x_1(t) + \alpha$$

$$\tilde{x}(t) = \text{speed dispersion}$$

Note that $\epsilon[\tilde{x}(t)] = 0$.

Substituting Eq. (41) into Eqs. (1), (2), and (3) yields

$$\dot{\tilde{x}}(t) = -(d)^{1/2}\left\{\frac{\cosh[(d)^{1/2}(T-t)]}{\sinh[(d)^{1/2}(T-t)]}\right\}\tilde{x}(t) - \left[\frac{1}{J} + \frac{1}{J(\omega_0^2 - d)}\left(a\omega_0 + d + (d)^{1/2}(a+\omega_0) \times \left\{\frac{\exp[-\omega_0(T-t)] - \cosh[(d)^{1/2}(T-t)]}{\sinh[(d)^{1/2}(T-t)]}\right\}\right)\right]\tilde{x}_2(t) \tag{42}$$

$$\dot{\tilde{x}}_2(t) = -\omega_0\tilde{x}_2(t) + \xi_w(t) \tag{43}$$

or in matrix form

$$\dot{\mathbf{z}}(t) = \mathbf{A}\mathbf{z}(t) + \mathbf{y}(t) \tag{44}$$

where

$$\mathbf{z}(t) \triangleq \begin{bmatrix} \tilde{x}(t) \\ \tilde{x}_2(t) \end{bmatrix}$$

$$\mathbf{y}(t) \triangleq \begin{bmatrix} 0 \\ \xi_w(t) \end{bmatrix}$$

and $\mathbf{A}$ is the coefficient matrix of Eqs. (42) and (43).

Let

$$\mathbf{Q}(t) = \epsilon[\mathbf{z}(t)\mathbf{z}^T(t)] \triangleq \begin{bmatrix} Q_{11}(t) & Q_{12}(t) \\ Q_{12}(t) & Q_{22}(t) \end{bmatrix} \tag{45}$$

Then it is known that the variance matrix $\mathbf{Q}$ satisfies the following differential equation:

$$\dot{\mathbf{Q}}(t) = \mathbf{A}\mathbf{Q}(t) + \mathbf{Q}(t)\,\mathbf{A}^T + \mathbf{y}(t)\,\mathbf{y}^T(t) \tag{46}$$

where superscript T denotes a matrix response. In this case $\mathbf{Q}(0) = 2 \times 2$ zero matrix.

The solution of Eq. (46) yields the following equations:

$$\dot{Q}_{11}(t) = -2(d)^{1/2}\left\{\frac{\cosh[(d)^{1/2}(T-t)]}{\sinh[(d)^{1/2}(T-t)]}\right\}Q_{11}(t) - \frac{2}{J}\left[1 + \frac{1}{(\omega_0^2 - d)}\left(a\omega_0 + d + (d)^{1/2}(a+\omega_0)\left\{\frac{\exp[-\omega_0(T-t)] - \cosh[(d)^{1/2}(T-t)]}{\sinh[(d)^{1/2}(T-t)]}\right\}\right)\right]Q_{12}(t) \tag{47}$$

$$Q_{11}(0) = 0 \tag{48}$$

$$\dot{Q}_{12}(t) = -\left(\omega_0 + (d)^{1/2}\left\{\frac{\cosh[(d)^{1/2}(T-t)]}{\sinh[(d)^{1/2}(T-t)]}\right\}\right)Q_{12}(t) - \frac{1}{J}\left[1 + \frac{1}{(\omega_0^2 - d)}\left(a\omega_0 + d + (d)^{1/2}(a+\omega_0)\left\{\frac{\exp[-\omega_0(T-t)] - \cosh[(d)^{1/2}(T-t)]}{\sinh[(d)^{1/2}(T-t)]}\right\}\right)\right]Q_{22}(t) \tag{49}$$

$$Q_{12}(t) = 0 \tag{50}$$

$$\dot{Q}_{22}(t) = -2\omega_0 Q_{22}(t) + 2\omega_0\sigma_c^2 \tag{51}$$

$$Q_{22}(0) = 0 \tag{52}$$

Let

$$R(t) \triangleq \epsilon[\tilde{u}^2(t)] \tag{53}$$

where $\tilde{u}(t) = u^*(t) - \epsilon[u^*(t)]$ and $u^*(t)$ is given by Eq. (38).

Hence,

$$R(t) = \left(\frac{k_b}{2} + \frac{k_t a}{2Jb} - \left[\frac{k_t (d)^{1/2}}{2Jb}\right]\left\{\frac{\cosh\left[(d)^{1/2}(T-t)\right]}{\sinh\left[(d)^{1/2}(T-t)\right]}\right\}\right)^2 Q_{11}(t) - \left(\frac{k_b}{2} + \frac{k_t a}{2Jb} - \left[\frac{k_t (d)^{1/2}}{2Jb}\right]\left\{\frac{\cosh\left[(d)^{1/2}(T-t)\right]}{\sinh\left[(d)^{1/2}(T-t)\right]}\right\}\right)$$

$$\times \left[\frac{k_t}{2J^2 b(\omega_0^2 - d)}\left(a\omega_0 + d + (d)^{1/2}(a+\omega_0)\left\{\frac{\exp\left[-\omega_0(T-t)\right] - \cosh\left[(d)^{1/2}(T-t)\right]}{\sinh\left[(d)^{1/2}(T-t)\right]}\right\}\right)\right] Q_{12}(t)$$

$$+ \left[\frac{k_t \sigma_c}{2J^2 b(\omega_0^2 - d)}\left(a\omega_0 + d + (d)^{1/2}(a+\omega_0)\left\{\frac{\exp\left[-\omega_0(T-t)\right] - \cosh\left[(d)^{1/2}(T-t)\right]}{\sinh\left[(d)^{1/2}(T-t)\right]}\right\}\right)\right]^2 \left[1 - \exp\left(-2\omega_0 t\right)\right] \quad (54)$$

III. Computer Results

A. System Parameters

The following parameters are arbitrarily chosen for the study of theoretical results in the digital computer:

$$J = 1.42 \text{ Nm/rad/s}^2$$

$$f = 0.825 \text{ Nm/rad/s}$$

$$k_b = 2.0 \text{ V/rad/s}$$

$$k_t = 2.0 \text{ Nm/A}$$

$$r = 1.0\ \Omega$$

B. Salient Features of the Solution

Figure 1 shows that the speed variance $Q_{11}(t)$ of Eq. (47) becomes zero at $t = T$. Hence, as $t \to T$, $\lim x(t) = \alpha$.

Control variance $R(t)$ [Eq. (54)] is bounded at $t = T$. It can be shown that if $x_2(t)$ is assumed to be stationary white-noise with zero mean, control variance becomes unbounded at $t = T$. When the stochastic optimal and stochastic sub-optimal [Eqs. (38) and (39), respectively] control laws are applied to the exact plant equations that are obtained by taking armature inductance into account and using an appropriate Monte Carlo Simulation technique (see Ref. 1), the corresponding results appear to be almost identical for a large numbers of Ts.

A sample of the corresponding results is shown in Fig. 2 for the case of speed control. Figure 3 shows a typical sample function of the Ornstein–Uhlenbeck process denoted by $x_2(t)$ and its corresponding terrain profile. During the Monte Carlo Simulation, response characteristics of the type shown in Fig. 2 are obtained for nine sample functions of the Ornstein–Uhlenbeck stochastic process along with their corresponding control energy

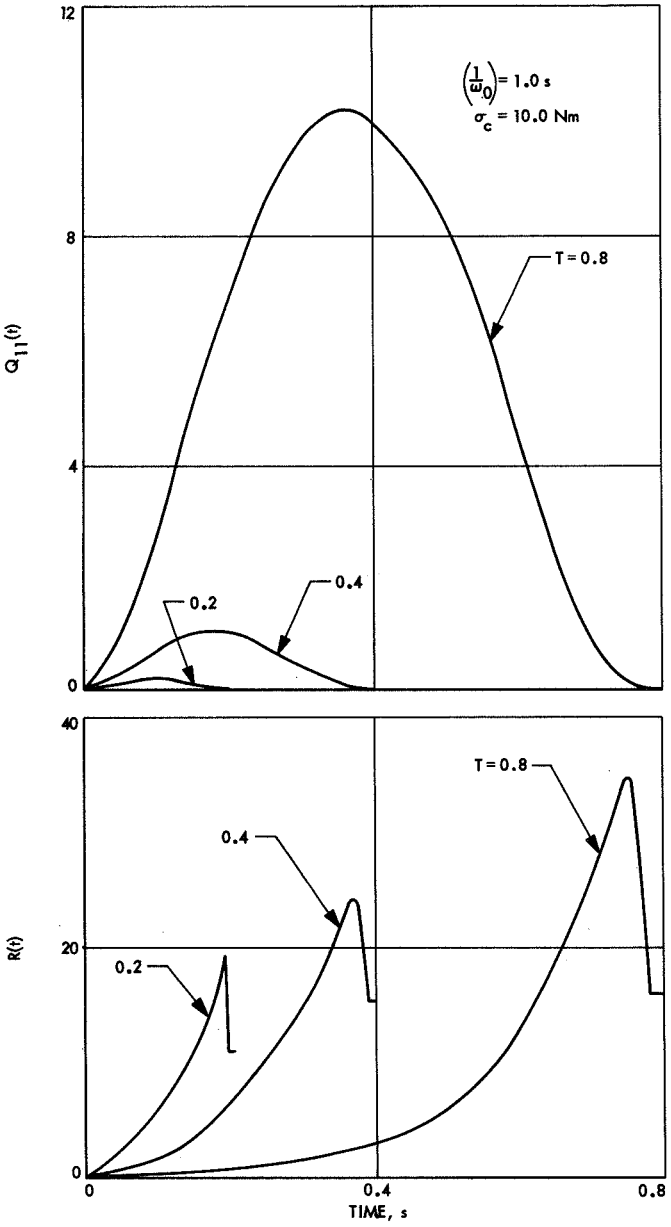

Fig. 1. Speed and control variances vs time

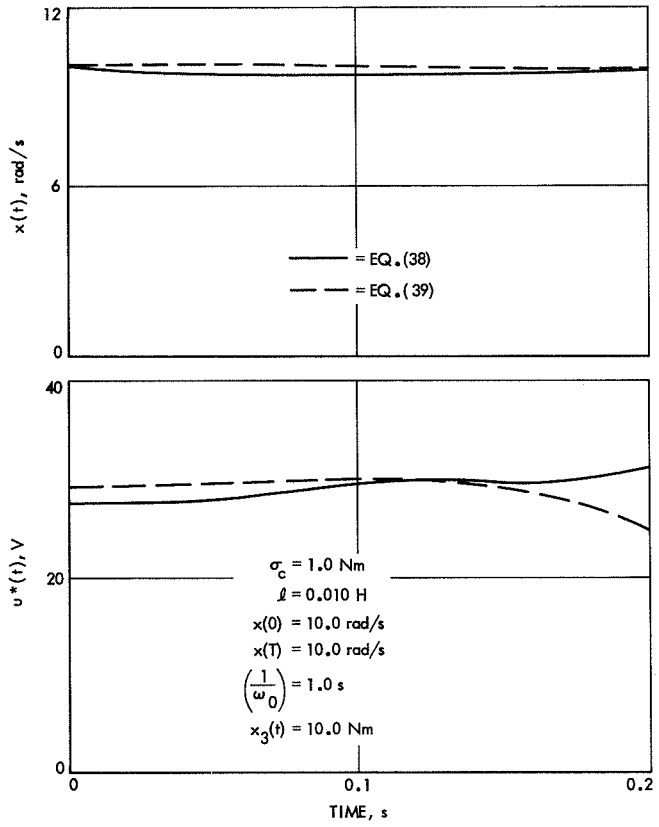

Fig. 2. Speed control solution

consumptions in $(0,T)$. All these results clearly indicate that $u^*(t) \cong u_{so}(t)$ without significantly degrading the performance characteristics of the system.

In this report Eq. (39) is called the minimum-energy control law whose mechanization is described in the subsequent paragraph. Figure 4 shows the comparison of the performance characteristics of the minimum-energy controller with those of a typical integral-type speed controller during the acceleration mode. In comparison with a typical proportional-type speed controller, the minimum-energy controller shows the electrical energy economy to be more by a factor of 10.0. However, during speed-control the minimum-energy controller operation does not show any significant advantage over the integral-type controllers. The comparison of performance characteristics of a minimum-energy controller with those of an integral-type controller is carried out under the assumption of

$$x_2(t) \equiv 0, \qquad 0 \leq t \leq T \tag{55}$$

Equation (55) indicates that the vehicle is moving on a terrain with constant-slope angle during the controlling period $(0,T)$. The details are given in Ref. 1 where it is also shown that if $v(t) \equiv \beta$ in $0 \leq t \leq T$ and the armature inductance of the motor is taken into account in the plant equations, the exact solution of the resulting optimization problem yields a dual-mode control law.

The dual-mode control law consists of only a bang-bang solution during the acceleration. Figure 5 shows the comparison between the performance characteristics of bang-bang and a minimum energy solution during the acceleration. The energy consumption of the bang-bang solution is about 3% less than that of the minimum-energy solution. However, the practical realization of

Fig. 3. A sample function of the Ornstein–Uhlenbeck process and its corresponding terrain profile

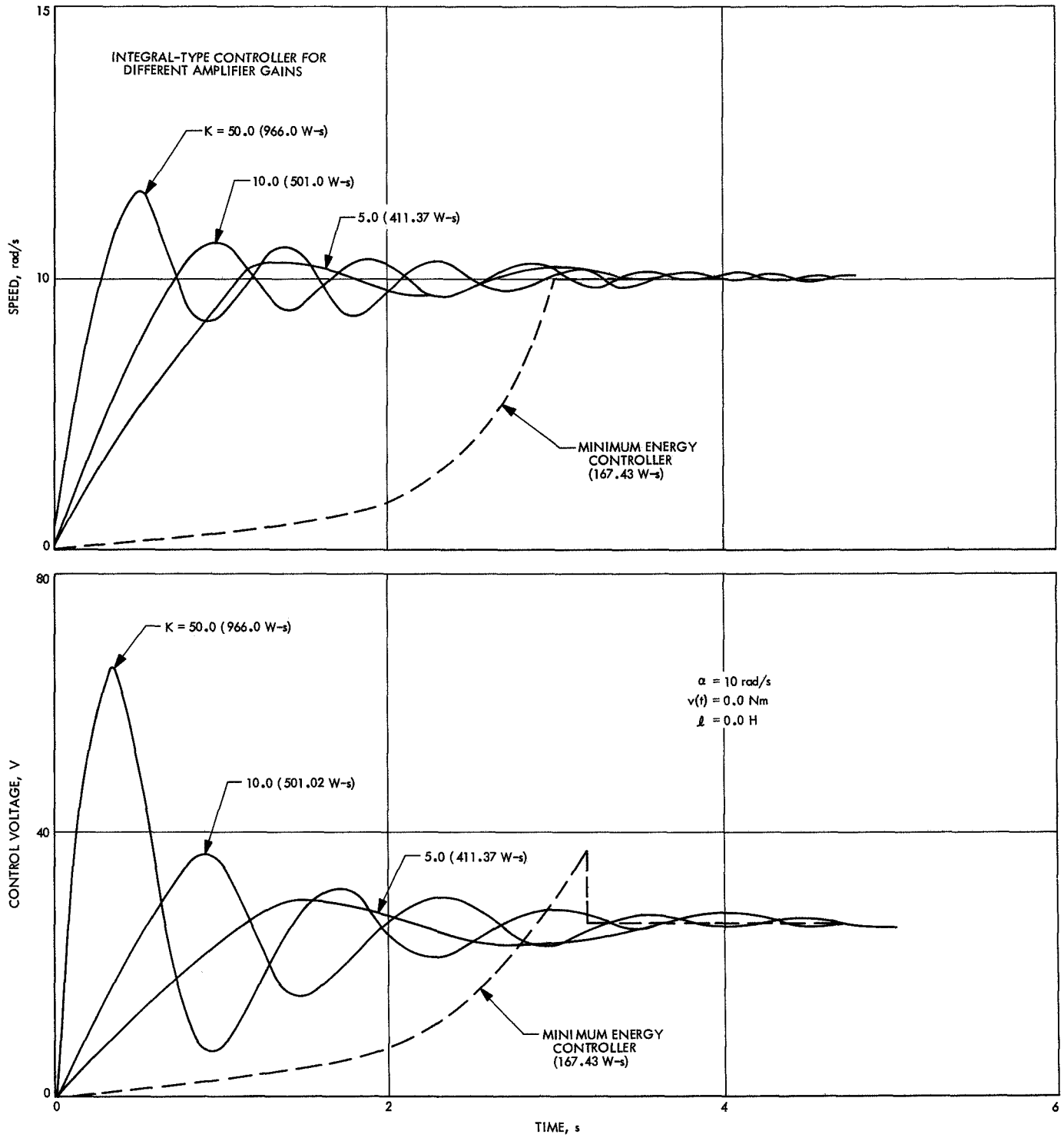

Fig. 4. Comparison of performance characteristics of the minimum-energy controller and the integral type speed controller

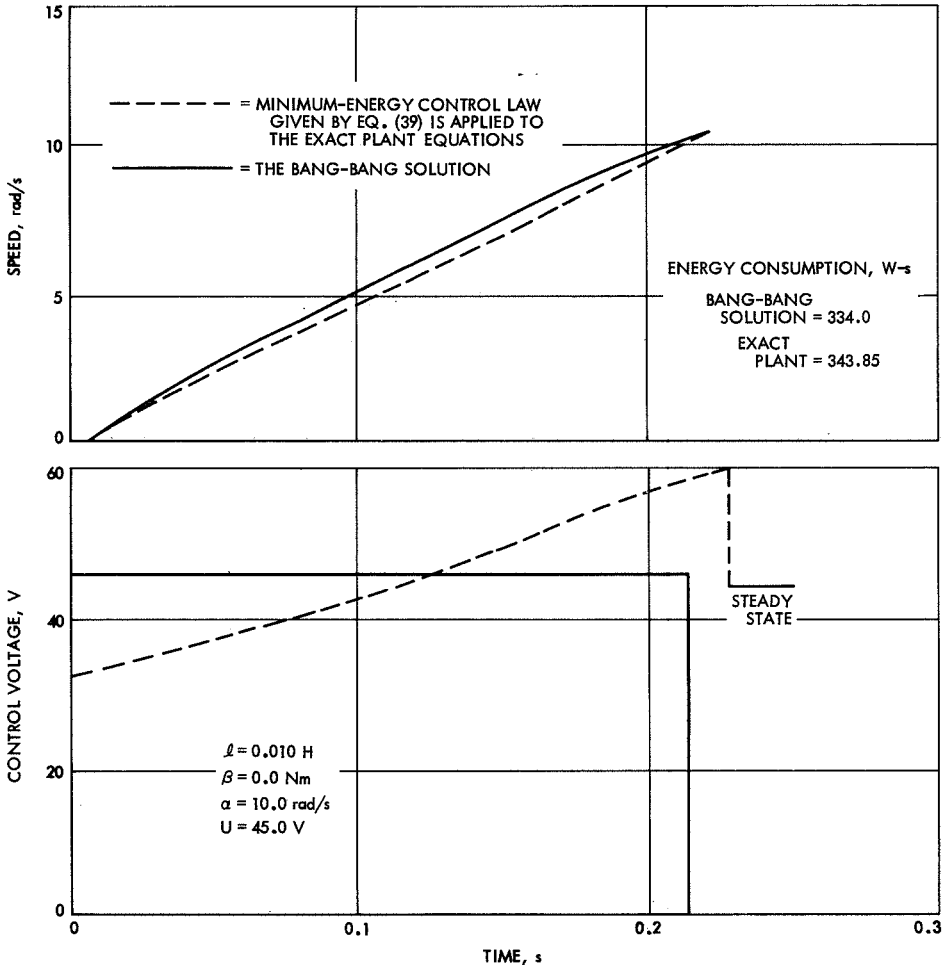

Fig. 5. Comparison of bang-bang solution with minimum-energy solution

dual-mode control law operation, that may consist of bang-bang and singular control laws in $0 \leq t \leq T$ for an infinite number of combinations between α and β, is extremely complex and expensive. Hence, the assumptions made on the removal of inequality constraints on $u(t)$ and armature inductance for reasons of mathematical simplicity yield an optimal system that can be easily and economically realized in practice. Selection of response time T requires the generation of computer results of the type shown in Fig. 6. The minimum-energy control law given by Eq. (39) adjusts the armature voltage of the motor in such a way that, even though $v(t)$ varies, it does not vary the speed of the vehicle. The computer results also yield some information on the correct choice of battery voltage for a particular system.

The minimum-energy control law, as described by Eq. (39), is a linear combination of feedback signals from: (1) a speed sensor (a tachometer-generator); (2) a terrain slope measuring device with a bias signal for tire resistance at zero speed (a pendulum-type device); and (3) a feed-forward signal from a throttle mechanism (a potentiometer). The functional relationship between the terrain slope $\phi(t)$ and the disturbance torque $v(t)$ for a wheeled-vehicle with rubber tires is given by

$$v(t) = [w_v \sin \phi(t) + f_1] \left(\frac{r_w c_F}{k_G}\right) \tag{56}$$

where

w_v = total weight of vehicle, lb

$\phi(t)$ = slope angle of terrain with respect to local horizontal, deg

f_1 = tire resistance at zero speed, lb

r_w = effective radius of wheel-time assembly, ft

k_G = gear ratio

c_F = conversion factor from ft-lb to Nm

IV. Mechanization of the Minimum-Energy Control Law

A. General Discussion

The control law described by Eq. (39) was mechanized in the laboratory of Section 344 of the Guidance and Control Division of the Jet Propulsion Laboratory. The system block diagram that corresponds to the one wheel drive system is shown in Fig. 7. In the laboratory the effects of terrain slope changes on the system dynamics are simulated by means of a second permanent-magnet dc motor (load motor), coupled directly to the drive motor shaft. The armature voltage of the load motor is controlled by a rheostat. If the armature voltage is higher than the back-emf voltage, the load motor generates a torque that opposes the motion of the drive motor, simulating the effect of terrain with a positive slope on the motion of the vehicle. If the armature voltage is less than the back-emf voltage, the load motor generates a torque that aids the motion of the drive motor, simulating the effect of terrain with a negative slope angle on the motion of the vehicle. A signal proportional to the direction and amplitude of armature current is then used to generate a signal for the second term in Eq. (39).

A pulse-width modulator determines the on and off times of control pulses to the silicon controlled rectifier (SCR) gates of step-down and step-up voltage converters according to the control law. The input signal to the pulse-width modulator is the sum of signals from the tacho-generator, disturbance-torque sensor, and acceleration and deceleration controller. The latter is called an optimal controller since it forces the system state to follow an optimal trajectory in $0 \leq t \leq T$. The pulse-width modulator activates the step-down or step-up voltage converters according to the output signal from the armature current-direction sensor.

The armature current-direction sensor generates its output signal by comparing the instantaneous values of minimum-energy control voltage and back-emf voltage. For example, if the minimum-energy control voltage is larger than the back-emf voltage, the pulse-width modulator activates the dc to dc SCR step-down voltage converter. At this time, the dc to dc SCR step-up voltage converter is automatically disabled and the battery supplies an electric current to the motor. If, on the other hand, the minimum-energy control voltage is less than the back-emf voltage, the pulse-width modulator activates the dc to dc step-up voltage converter. During this period the dc to dc step-down voltage converter is automatically disabled and the motor supplies electric current to the battery.

The optimal controller feeds an acceleration or deceleration signal with the desired response time T to the input circuit of the pulse-width modulator. The response time T is automatically adjusted for any acceleration or deceleration control action according to indicated computer results of the type shown in Fig. 6.

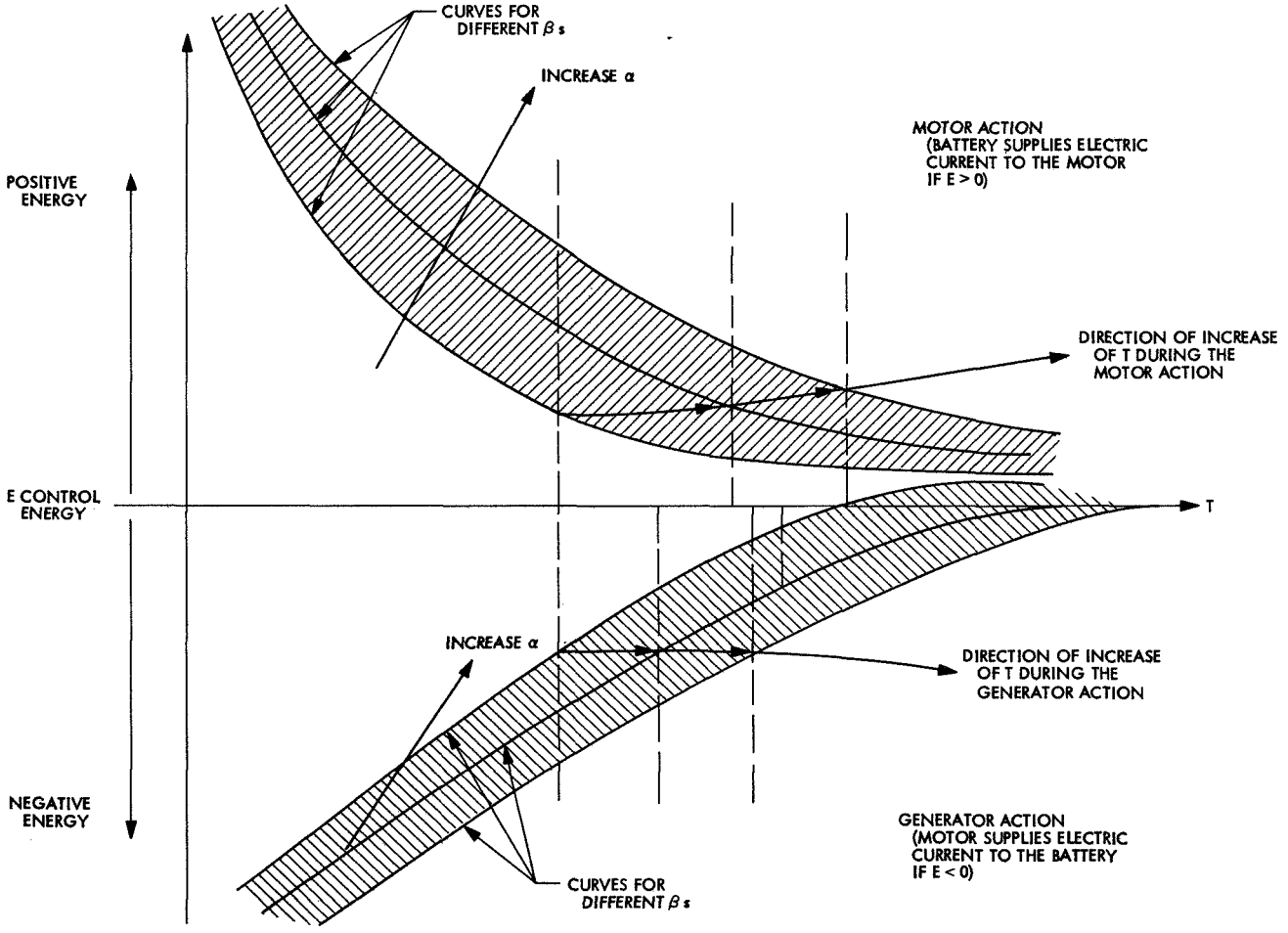

Fig. 6. Selection of response time T [x(0) = 0.0]

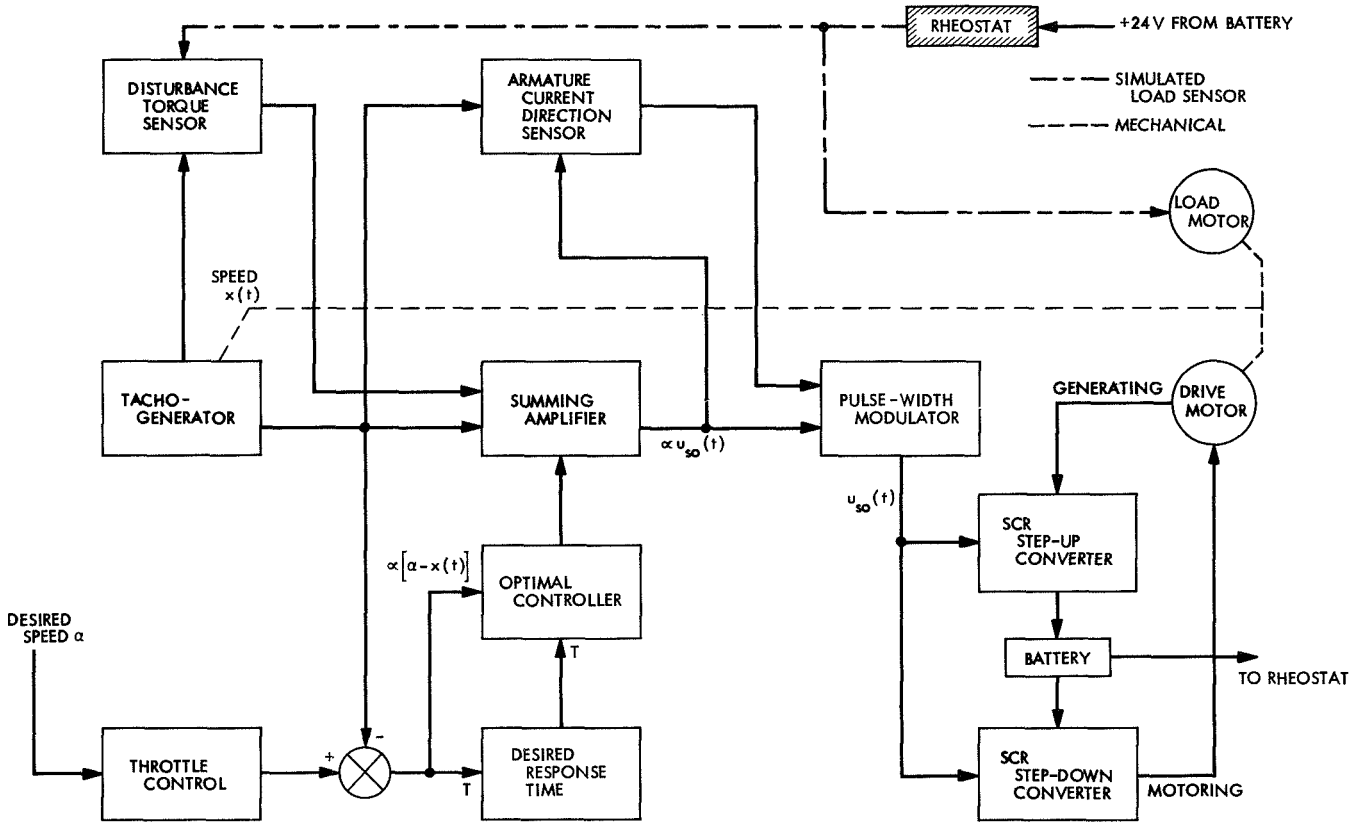

Fig. 7. Minimum-energy control system block diagram

The tacho-generator speed sensor feeds a signal to the input circuit of the pulse-width modulator proportional to the speed of the vehicle as specified by the control law. The pulse-width modulator input circuit also applies signals to the armature current-direction sensor, the optimal controller, and the disturbance-torque sensor.

B. Design and Development of Control Circuits

1. Optimal controller. The primary function of the optimal controller is to respond to signals from the throttle setting mechanism (desired speed), and the tacho-generator speed sensor (actual), and to accelerate or decelerate the motor speed to the desired speed setting in an optimal manner. The throttle setting mechanism also automatically sets the desired response time for the minimum-energy controller. The output signals from the optimal controller for acceleration or decleration of the vehicle are applied to the base circuit of transistor T39 in the pulse-width modulator. Whenever the desired speed is reached $[x(t) = \alpha]$, as explained in Ref. 1, the output signals of the optimal controller cease (become identically zero) until a new desired speed setting is applied to the system. Figure 8 shows the final values of circuit elements for the optimal controller which were determined by using standard analytical tools.

Whenever $[\alpha - x(t)] > 0$ a schmitt-trigger circuit supplies a voltage (10 V) through transistor T7 to transistors T8 and T9. Transistor T9 then supplies a current proportional to $[\alpha - x(t)]$ to point PA that is connected to the base circuit of transistor T39 in the pulse-width modulator. Whenever $[\alpha - x(t)] < 0$, another schmitt-trigger circuit supplies voltage (10 V) through transistor T13 to transistors T14 and T15. Transistor T15 then draws a current proportional to $[\alpha - x(t)]$ from point PD, also connected to the base circuit of transistor T39 in the pulse-width modulator. The collector voltage value of transistor T2 at $t = 0$, in response to a throttle setting position, determines the response time in a required speed setting control action.

2. Tacho-generator speed sensor. The primary function of the speed sensor (tacho-generator) is to measure the speed of the dc motor and provide this information to establish steady-state operation for the minimum-energy

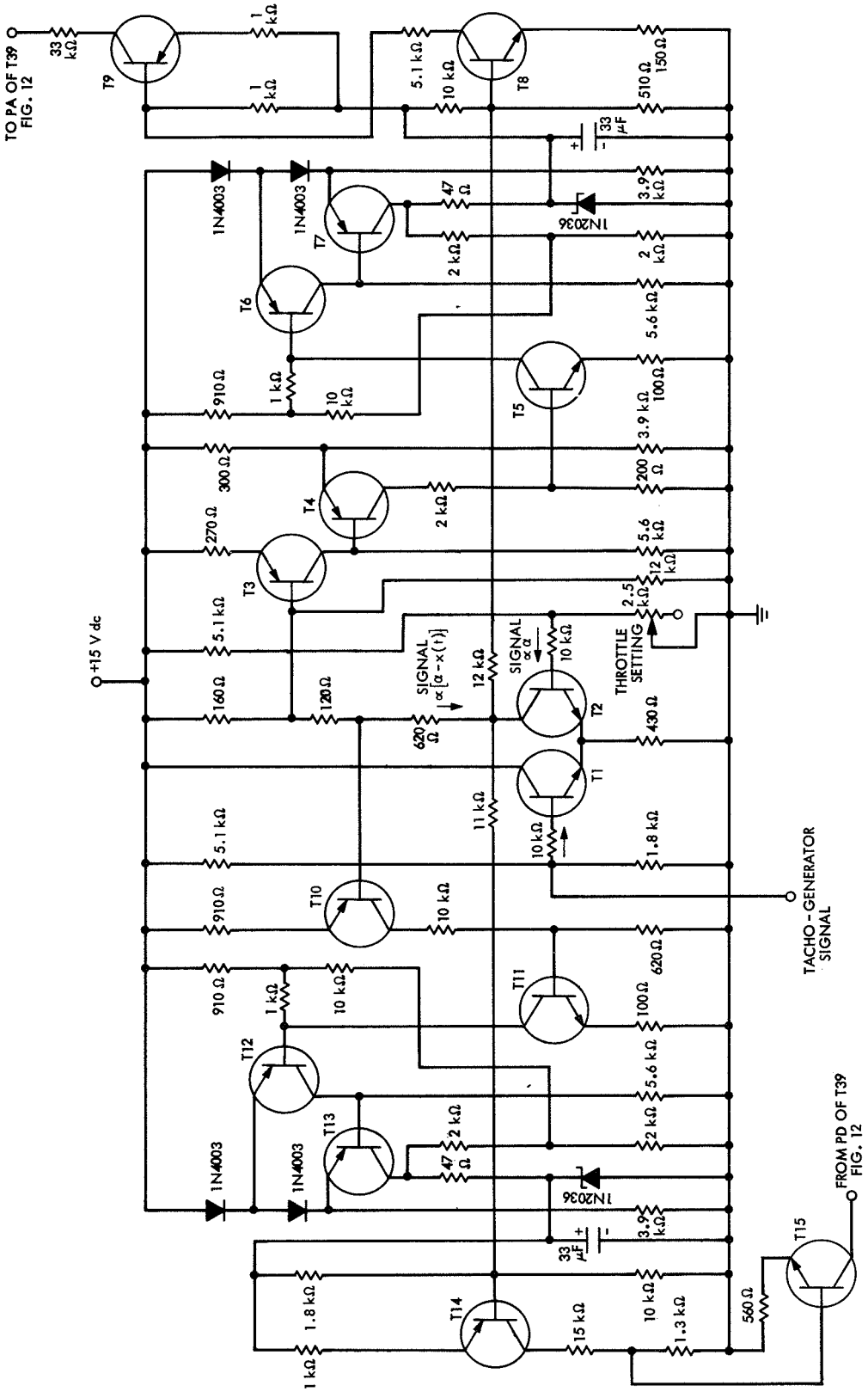

Fig. 8. Optimal controller

controller. The motor speed is measured by a tacho-generator connected to the motor shaft by means of a pulley-belt. The tacho-generator output signal is applied to three transistor amplifier stages. One transistor amplifier stage produces a variable pulse width output according to the steady-state form of the optimal control law during the motoring and generating modes of operation. The output is applied to the input circuit of the pulse-width modulator (base of transistor T39) and the armature current-direction sensor (base of transistor T28).

A second transistor amplifier stage converts the tacho-generator input to an output signal proportional to the back-emf voltage of the dc motor. This signal in conjunction with the optimum control law signal produces a difference voltage that determines the mode of operation (and is explained further in this report).

The tacho-generator output is also fed to a third transistor amplifier stage that provides an input to the optimal controller. The optimal controller compares this signal with that from the throttle setting circuit and produces a difference voltage. The difference voltage is used to turn-on or turn-off the voltage supply for the acceleration or deceleration control circuits of the optimal controller.

Figure 9 shows the final values for circuit elements of the speed sensor that were determined by using standard analytical tools. The tacho-generator is a very small permanent-magnet dc motor coupled to the drive motor shaft by means of a pulley-belt and connected in a balanced bridge circuit. The tacho-generator output voltage is linearly related to the motor speed from 0 V to a maximum speed voltage level. This signal is applied to the base circuit of transistor T16 as shown in Fig. 9.

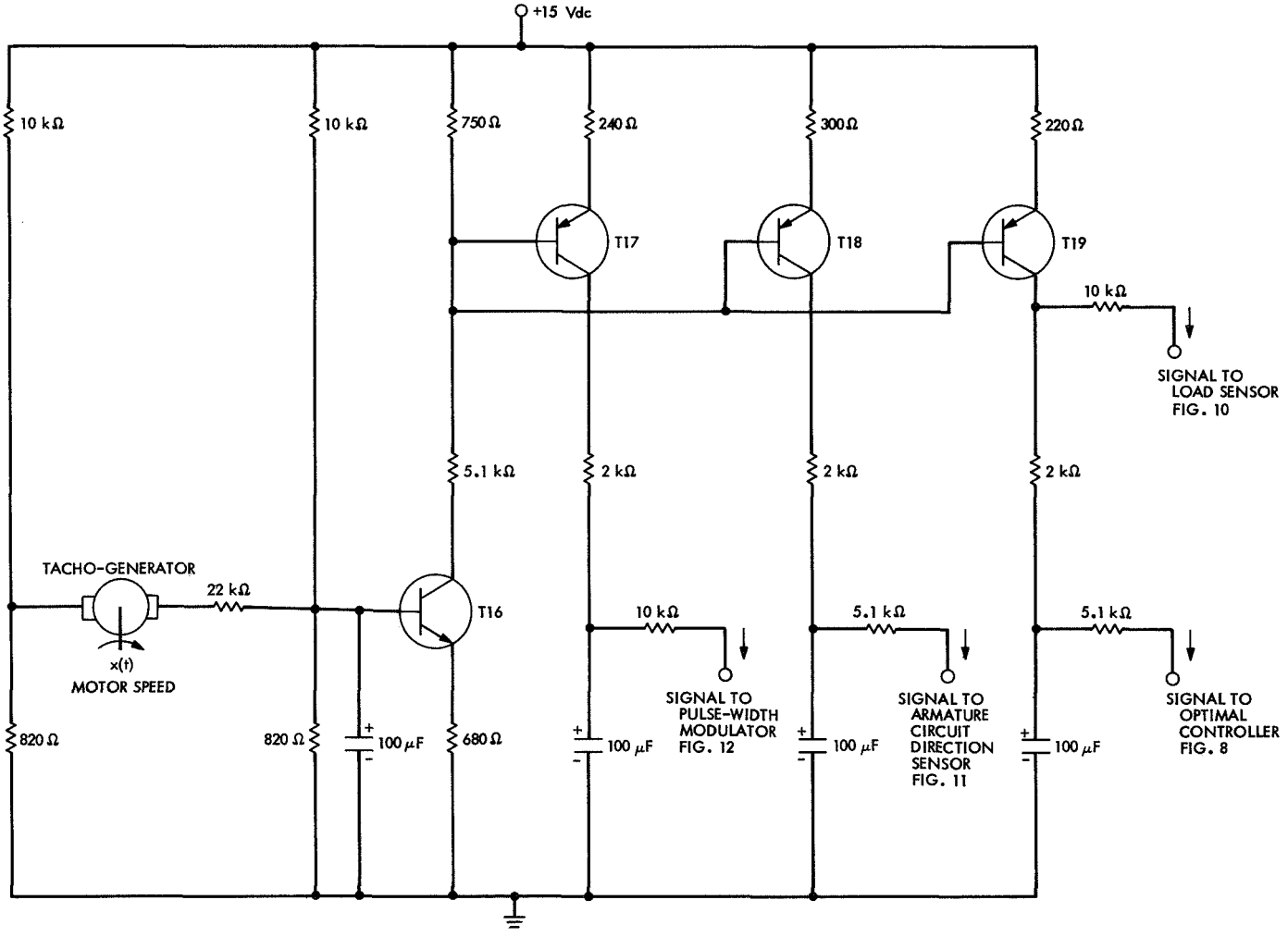

Fig. 9. Speed sensor

Transistors T17, T18, and T19 transfer this speed information to the pulse-width modulator, the armature current-direction sensor, the optimal controller, and load sensor. The noise produced by the brush-commutator action of the tacho-generator is minimized by the use of resistance-capacitance networks.

3. Simulated load sensor. In practice the disturbance torque $v(t)$ is measured by a pendulum-type device. The signal produced is directly proportional to the magnitude and polarity of the terrain slope angle with respect to local horizontal direction. This signal is applied to the input circuit of the pulse-width modulator. As shown in Ref. 1, this prevents any change in the vehicle speed from its desired value under the influence of terrain slope changes. In the laboratory this operation is simulated with the circuit shown in Fig. 10. The rheostat applies a voltage to the armature circuit of the load motor that is mechanically connected to the drive motor shaft. If the armature voltage is greater than the back-emf voltage in the load motor, its output torque opposes the motion of the drive motor. This action simulates the effect of a positive terrain slope on the motion of the vehicle. If the armature voltage is less than the back-emf voltage in the load motor, its output torque aids the motion of the drive motor. This action simulates the effect of a negative terrain slope on the motion of the vehicle.

The back-emf voltage of the load motor is measured by using the speed signal from the tacho-generator since they are rotating at the same speed and the back-emf constant of the load motor is known.

The differential amplifier, composed of transistors T20 and T21, responds to signals proportional to back-emf and armature voltages of the load motor in the following manner:

(1) When the armature voltage is larger than the back-emf voltage in the load circuit, transistor T24 is turned on and transistor T27 is turned off. Transistor T24 supplies a current proportional to the difference between armature and back-emf voltages to the base circuit of transistor T39 in the pulse-width modulator in such a way that, even though the vehicle encounters a terrain with a positive slope angle, vehicle speed remains constant at its desired speed setting.

(2) When the armature voltage is less than the back-emf voltage in the load circuit, transistor T27 is turned on and transistor T24 is turned off. Transistor T27 draws a current proportional to the difference between the armature and back-emf voltages from the base circuit of transistor T39 in the pulse-width modulator in such a way that when the vehicle encounters a terrain with a

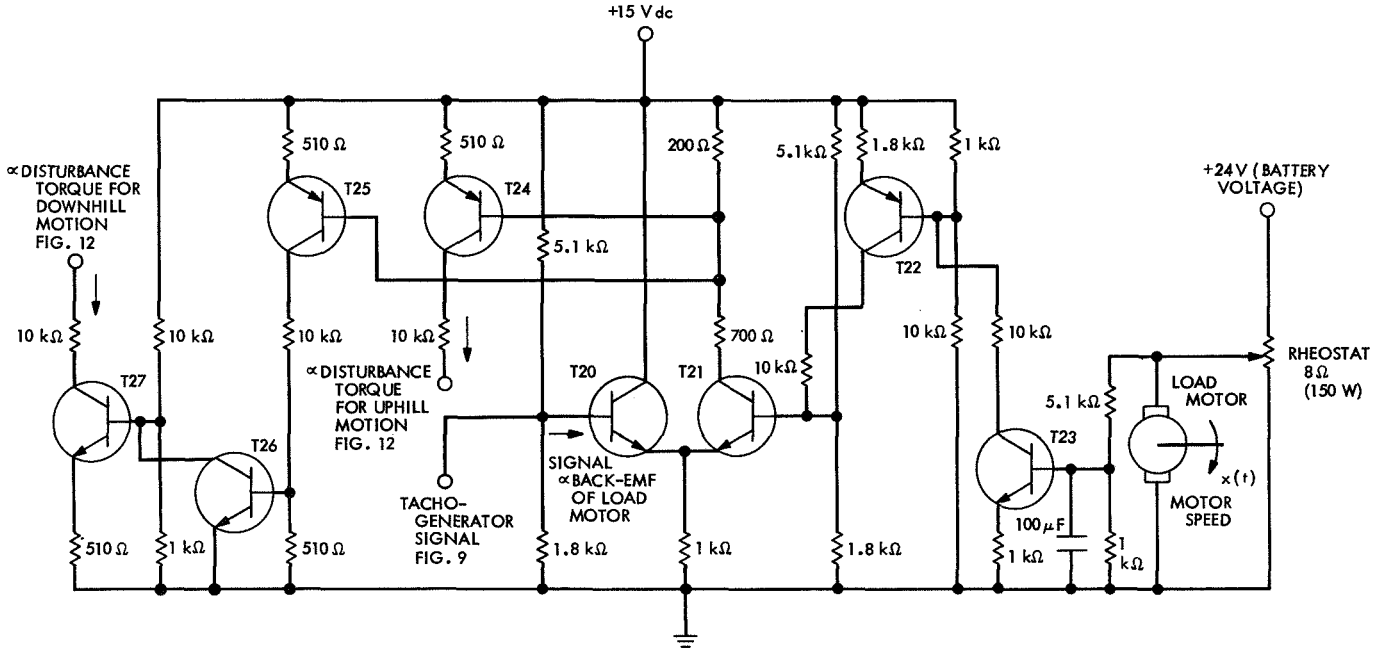

Fig. 10. Simulated load sensor

negative slope angle its speed remains at its desired setting.

It has been assumed that the inductance in the load motor armature circuit is negligible. Hence, the armature current that is proportional to the output torque of the load motor is indicated by the difference between the armature and back-emf voltages.

4. *Armature current-direction sensor.* The armature current-direction sensor controls the mode of operation for the pulse-width modulator. It consists of a comparator circuit and two schmitt-trigger circuits. The schmitt-trigger circuits turn the voltage supply to one of the control circuits of the pulse-width modulator on or off, depending on the polarity of the error signal between the samples of the optimal-control and back-emf voltages. The only requirement of the armature current-direction sensor is to provide a dead-band between the positive- and negative-error signals. The presence of this dead-band eliminates the possibility of a short circuit across the battery terminals when the mode of operation in the system changes from motoring to generating or vice versa. The final values of the circuit elements for the armature current-direction sensor are shown in Fig. 11.

5. *Pulse-width modulator.* The pulse-width modulator contains two identical SCR gate circuits. The motoring mode circuit is identified as the first channel and the generating mode circuit as the second channel. The primary function of the pulse-width modulator is to supply firing signals to the SCR gate circuits of the dc to dc voltage converters. These firing signals ensure that the armature voltage of the motor is controlled according to the optimal-control law during the motoring and generating modes of operation. The operation of the motor in the motoring or generating mode depends on the difference between the instantaneous values of the optimal-control and back-emf voltages. When the optimal-control voltage becomes greater than the back-emf voltage, the armature current-direction sensor switches on the voltage supply for the control circuit of the first channel of the pulse-width modulator that in turn activates the motoring mode of operation. The voltage supply for the control circuit of the second channel (generating mode) of the pulse-width modulator is switched off automatically. Conversely, when the optimal-control voltage becomes less than the back-emf voltage, the armature current-direction sensor switches the voltage supply on for the control circuit of the second channel of the pulse-width modulator that activates the generating mode of operation. The voltage supply for the control circuit of the first channel (motoring mode) of the pulse-width modulator is switched off automatically.

The requirements to be satisfied by the pulse-width modulator are determined from the design considerations of the dc to dc voltage converters. The requirements are:

(1) Pulse frequency, 250 Hz.

(2) Minimum pulse-width, 400 μs; maximum pulse-width, 3.6 ms.

(3) Maximum firing signal to SCR gate circuits, 6.8 V; maximum current to SCR gate circuits, 40 MA.

(4) Nominal pulse width of the firing signal to SCR gate circuits, 20 μs at 6.8 V.

(5) The input voltage to the pulse-width modulator is related to the conduction duration of the main SCR by a linear relationship.

The signals from the optimal controller, tacho-generator and simulated load sensor are fed to the input circuit of the pulse-width modulator as shown in Fig. 12. The input circuit output is simultaneously fed to the input circuits of the motoring and generating channels of the pulse-width modulator as shown in Figs. 13 and 14, respectively.

In the design of the pulse-width modulator, the procedure of the subsequent paragraphs has been used for each portion of the pulse-width modulator.

A unijunction relaxation oscillator (Ref. 2) generates a sawtooth waveform with a stable frequency of 250 Hz and a peak amplitude of 6.8 V. This is accomplished by charging the 0.1 μF capacitor with constant current from the collector circuit of a transistor. The capacitor voltage is applied to the base circuit of a transistor whose emitter bias is linearly proportional to the minimum-energy control voltage. When the amplitude of the capacitor voltage exceeds the amplitude of the emitter bias voltage of the transistor, within the period of relaxation oscillation, a schmitt trigger generates a pulse in the primary winding of the pulse transformer. The secondary winding of the pulse transformer in the motoring channel of the pulse-width modulator is connected to the gate circuit of the main SCR of the dc to dc voltage step-down converter. The secondary winding of the pulse transformer in the generating channel of the pulse-width modulator is connected to the gate circuit of the commutating SCR of the dc to dc voltage step-up converter.

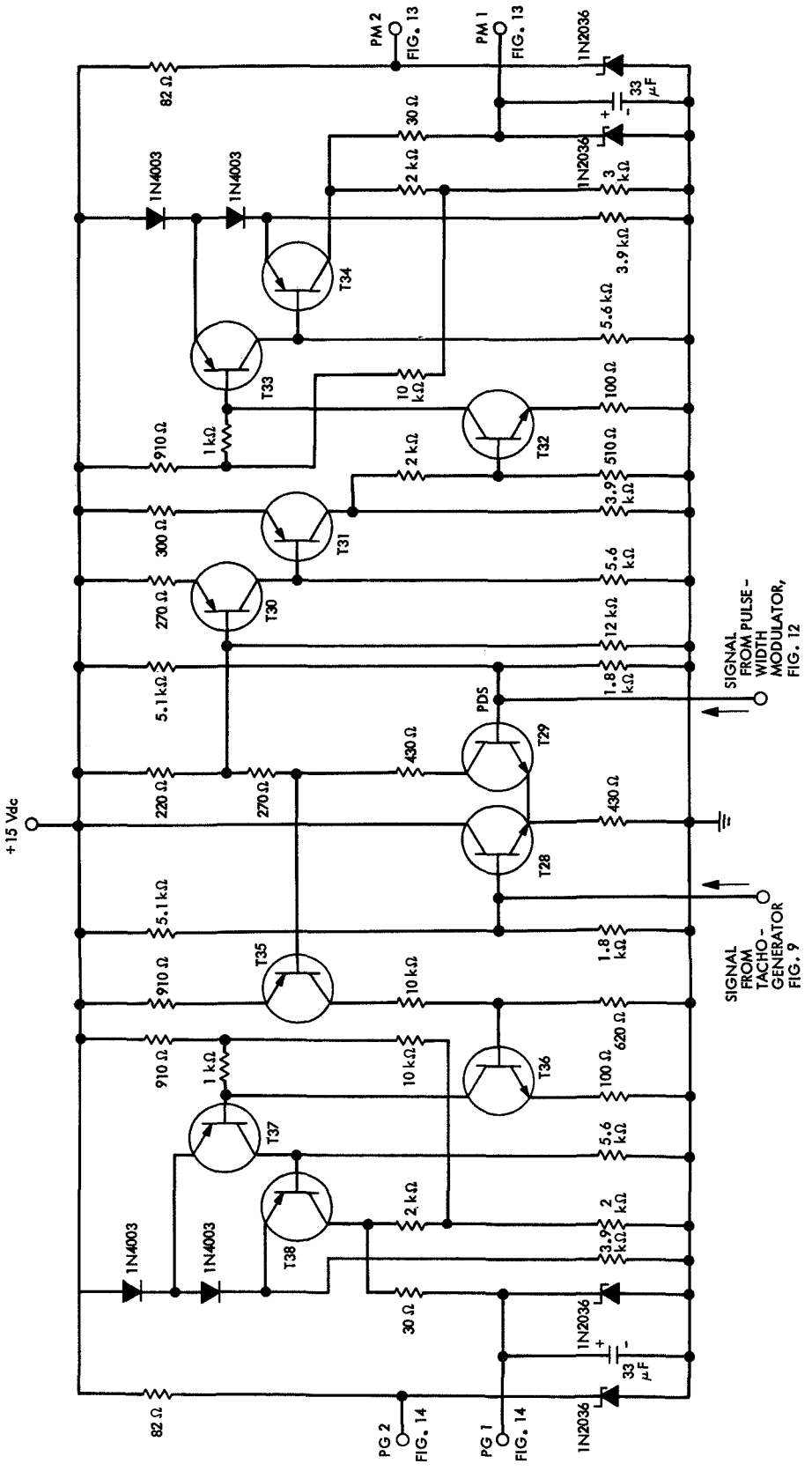

Fig. 11. Armature current-direction sensor

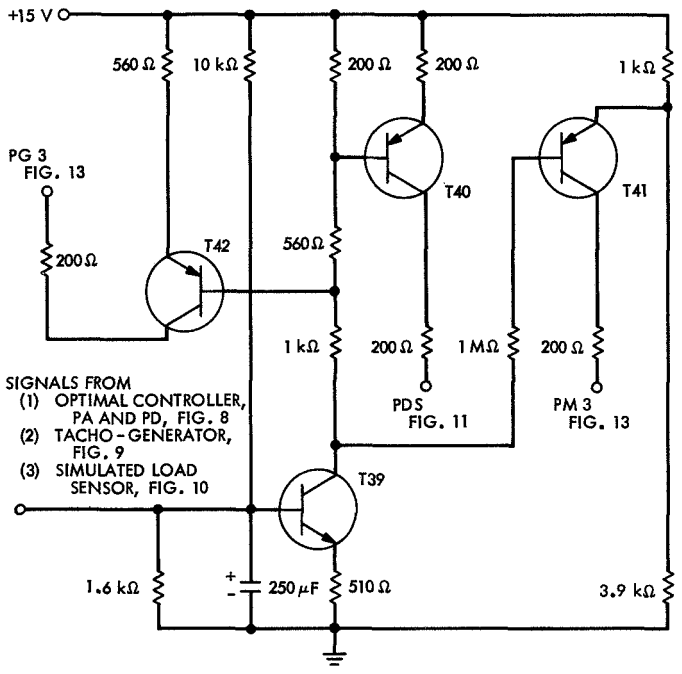

Fig. 12. Input circuit of the pulse-width modulator

A schmitt trigger, controlled by the schmitt trigger of the control circuit described in the previous paragraph, is designed to generate the desired firing pulses for the commutating SCR of dc to dc step-down voltage converter and the main SCR of dc to dc step-up voltage converter. The firing/timing operation of the pulse-width modulator is shown in Fig. 15 for two particular idealized conditions.

6. The SCR dc to dc voltage converters. The SCR dc to dc step-down and step-up voltage converters (Ref. 3) are controlled by the pulse-width controller according to the minimum-energy control law. The SCR step-down voltage converter is controlled by the motoring channel and SCR step-up voltage converter is controlled by the generating channel of the pulse-width modulator. As mentioned previously, the mode of operation is imposed on the pulse-width modulator by the armature current-direction sensor. During the motoring mode of operation the battery supplies a current to the motor armature circuit and during the generating mode of operation the battery is charged with a current from the motor armature circuit. Figure 16 shows the configuration of the SCR dc to dc converters.

The main SCR of the dc to dc step-down voltage converter (SCR 1) supplies the required electric current from the battery into the armature circuit whenever a signal v_{T_1} of appropriate duration and amplitude is applied from the pulse-width modulator to its gate circuit. The SCR 1 is turned off by SCR 2 which applies a voltage pulse across SCR 1 in the reverse direction. The amplitude of the voltage pulse (with respect to ground potential) is approximately equal to twice the value of the battery voltage. This commutation, or turn-off action of SCR 1, is accomplished by the operation of a resonant commutation circuit consisting of L1, D1, C1, and SCR 2. At the end of the commutation action, SCR 1 regains its blocking ability and is ready to be turned on by v_{T_1} in the next cycle. By adjusting the duration of turn-on and turn-off times of SCR 1 within the pre-specified period of operation, it is possible to vary the average voltage across motor terminal T1 and T2 as shown in Fig. 16, according to a control law. The average voltage between terminals T1 and T2 is always less than the battery voltage E_b.

The gate signals v_{T_3} and v_{T_4} are turned off by the automatic action of the armature current-direction sensor. The main SCR of the dc to dc step-up voltage converter (SCR 3) transfers the required current from the motor armature circuit into the battery whenever a signal v_{T_3} is applied from the pulse-width modulator to its gate circuit. The gate signals v_{T_1} and v_{T_2} are turned off by the automatic action of the armature current-direction sensor. The SCR 3 is turned off by SCR 4 which applies a voltage pulse across SCR 3 in the reverse direction. The amplitude of the voltage pulse, with respect to the anode potential of SCR 3, is approximately equal to the motor armature voltage. This commutation action is accomplished by capacitor C2 and SCR 4.

At the end of commutation action, SCR 3 regains its blocking ability and is ready to be turned on by v_{T_3} in the next cycle. By adjusting the duration of turn-on and turn-off times of SCR 3, within pre-specified period of operation, it is possible to vary the average voltage across the primary winding of the step-up transformer, shown in Fig. 16, according to a control law. This voltage is always less than the back-emf voltage of the motor.

Capacitor CF is the filter capacitor that tends to stabilize the source voltage level. Diode D2 prevents the charging of capacitor C1 by the back-emf voltage of the motor during the regenerative braking control action. Diode D3 provides a continuous current flow to the armature circuit during the motoring mode of operation. Battery voltage E_b is switched on and off across armature terminals T1 and T2 in such a way that the average value of the armature voltage approximates the value of voltage given by the minimum-energy control law.

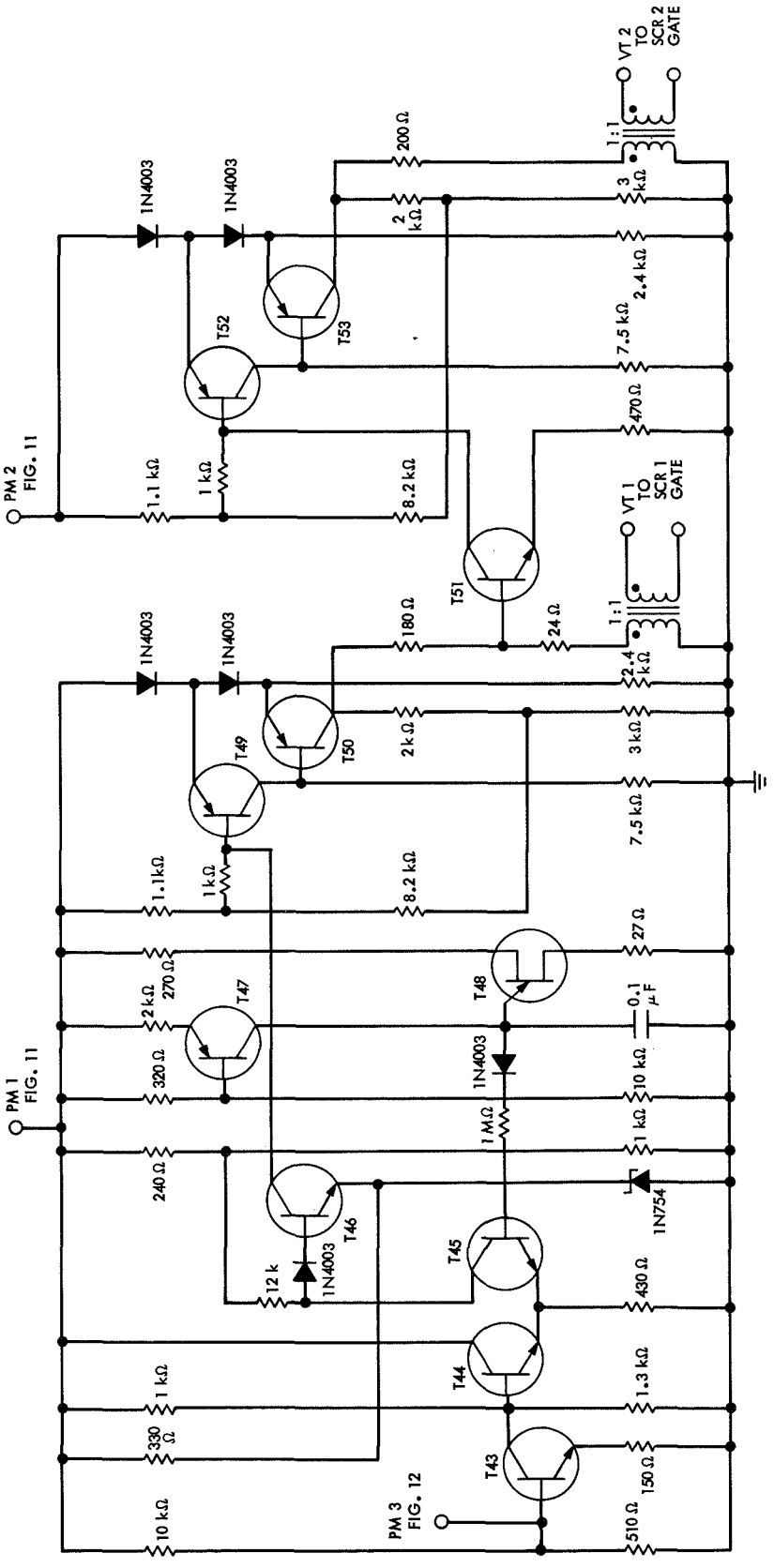

Fig. 13. Motoring channel of the pulse-width modulator

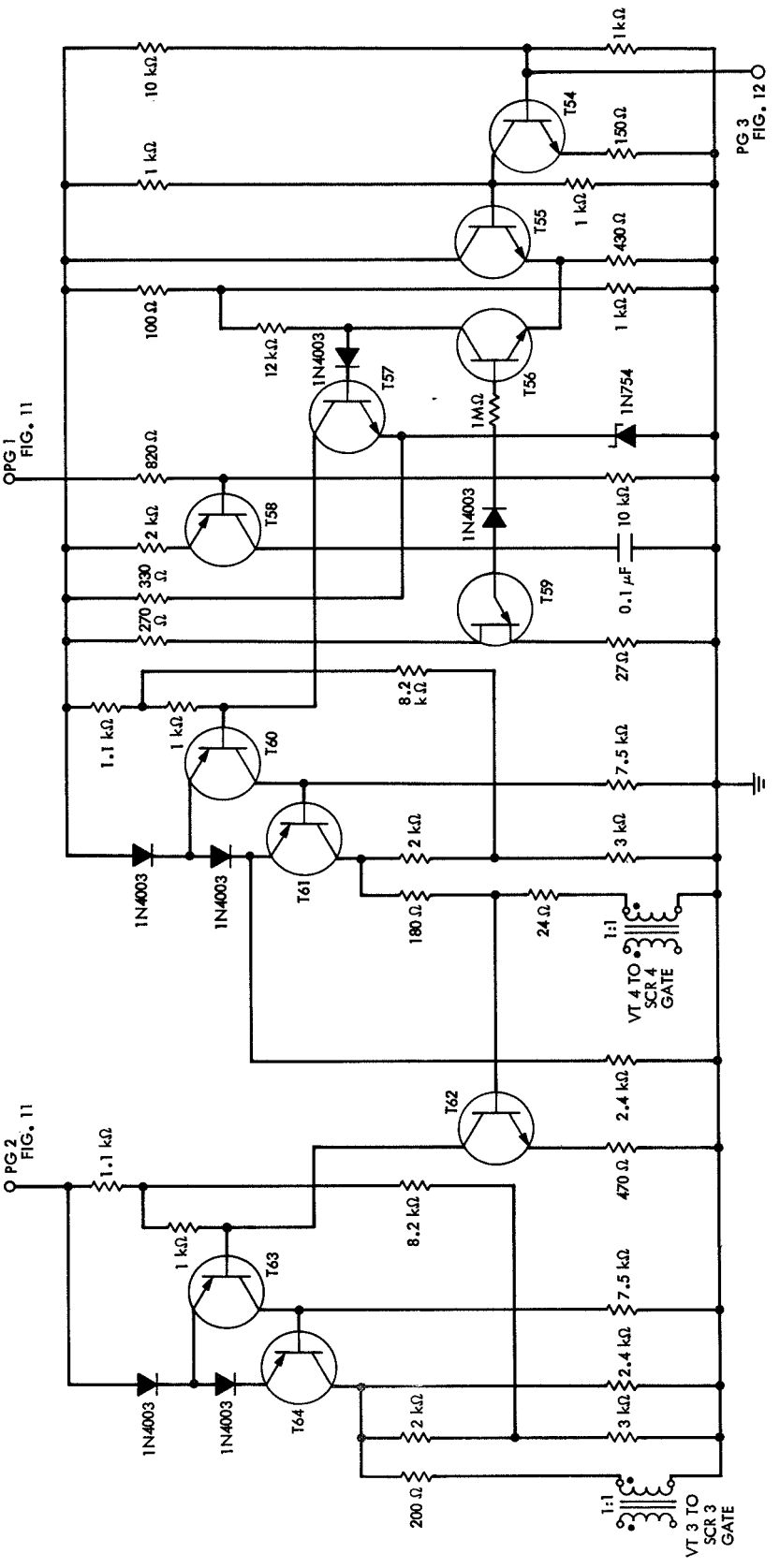

Fig. 14. Generating channel of the pulse-width modulator

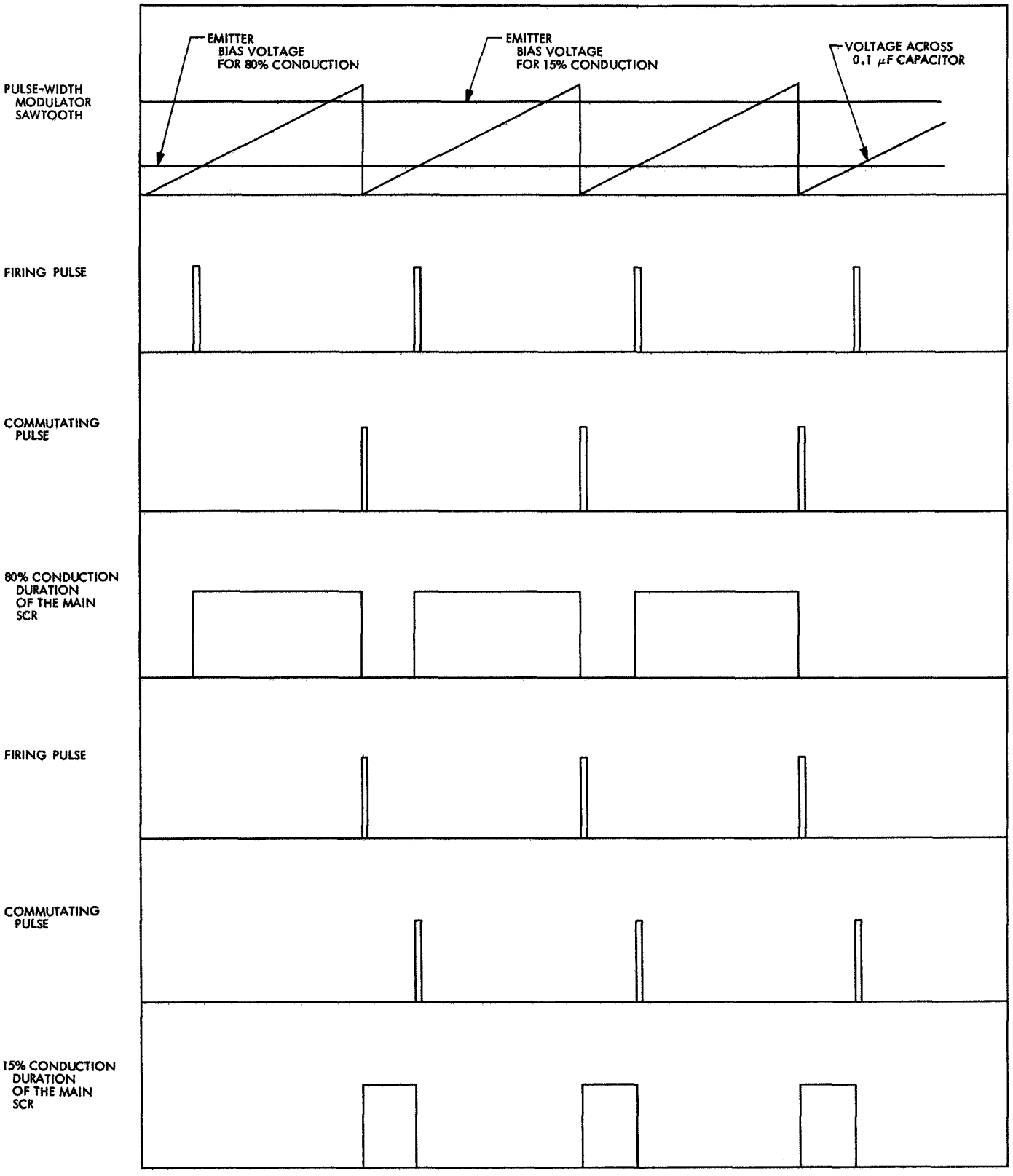

Fig. 15. Pulse-width modulator ideal characteristics

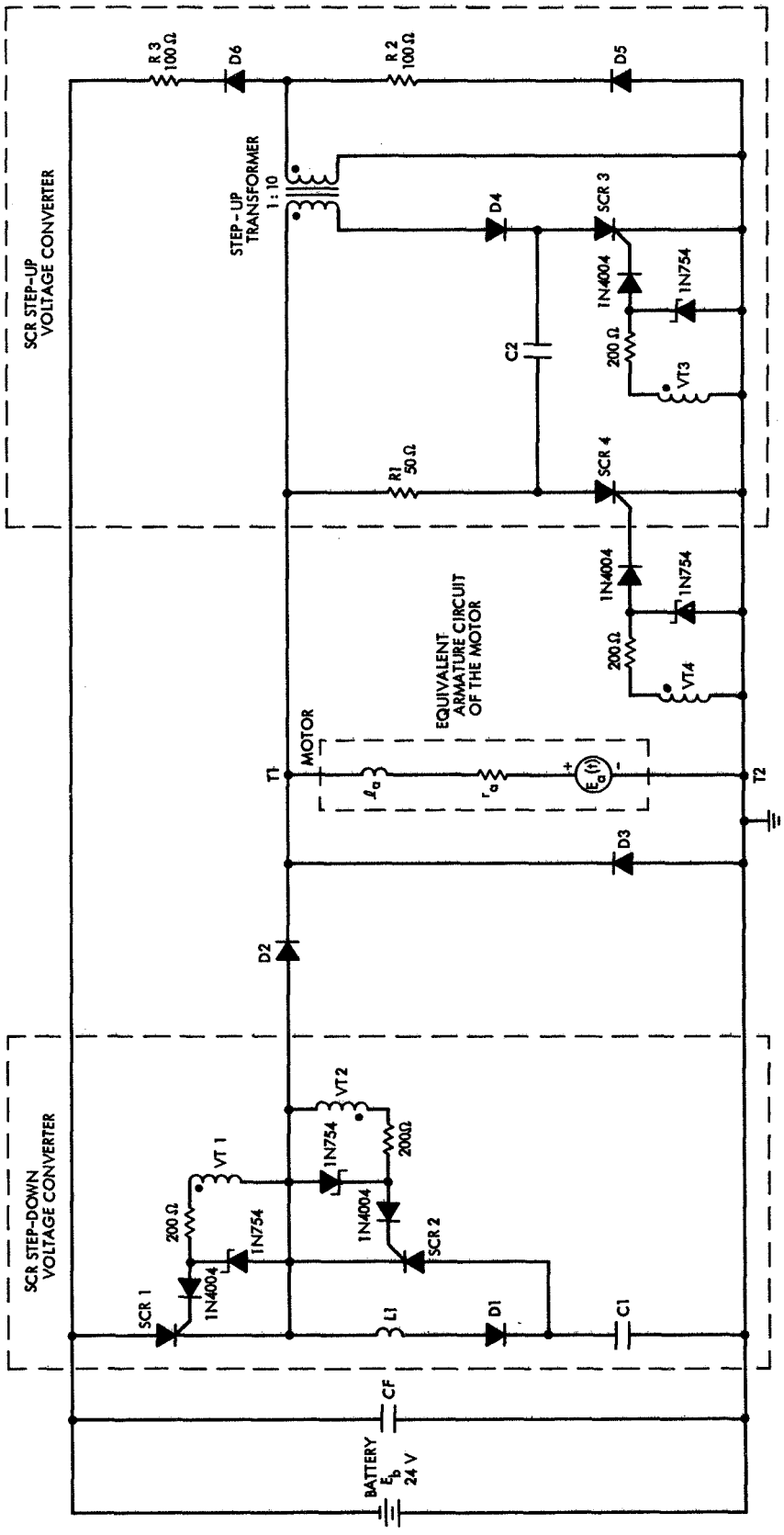

Fig. 16. The SCR dc to dc voltage converters of the minimum-energy controller

The equivalent armature circuit of the motor is assumed to have a constant dc resistance r_a, a constant inductance ℓ_a, and a voltage generator E_a, or back-emf voltage that is linearly proportional to the speed of the motor.

A step-up transformer charges the battery from a prespecified minimum value of back-emf voltage during the regenerative braking. Diode D4 prevents oscillations between C2 and the primary winding inductance of the step-up transformer during a cycle.

Diode D5 is the free-wheeling diode for the step-up transformer circuit. The primary function of diode D5 is to prevent the occurrence of extremely high voltages whenever SCR 3 is turned off during the regenerative control action. During the time interval when SCR 3 is off, the energy stored in the transformer windings is dissipated across resistor R2.

Diode D6 provides a unidirectional current flow from the motor armature circuit into the battery during the time interval when SCR 3 is conducting.

a. Design parameters for step-down converter. The design parameters of the SCR dc to dc step-down voltage converter are obtained as described in the subsequent paragraphs.

To obtain the first design parameter, consider that SCR 1 is turned on by the application of a gate signal v_{T_1}. By assuming initial conditions of zero current in L1 and zero voltage across C1 and applying standard methods to the commutating circuit of SCR 1, the following equations apply:

$$i_{C_1}(t) = \left(\frac{E_b}{L_1\omega}\right) \exp(-\alpha t) \sin \omega t \tag{57}$$

$$v_{C_1}(t) = E_b[1 - \exp(-2\alpha t) \cos \omega t] - E_b\left(\frac{\alpha}{\omega}\right) \exp(-\alpha t) \sin \omega t \tag{58}$$

where

$i_{C_1}(t) \triangleq$ instantaneous value of the charging current of capacitor C1

$v_{C_1}(t) \triangleq$ instantaneous value of the voltage across capacitor C1

$r_c \triangleq$ dc resistance of diode D1, assumed to be constant

$$\alpha \triangleq \frac{r_c}{2L_1}$$

$$\omega^2 \triangleq \left(\frac{1}{L_1C_1} - \frac{r_c^2}{4L_1^2}\right)$$

In the derivation of Eqs. (57) and (58), it has been assumed that when SCR 1 is turned on, the battery current primarily flows through L1 and D1 to C1 over the charging interval, which for practical reasons is 100–200 μs. This is justified since $\ell_a \gg L_1$. Furthermore, if α is also small then $\exp(-\alpha t) \approx 1.0$. Hence, Eqs. (57) and (58) become

$$i_{C_1}(t) \cong \left(\frac{E_b}{L_1\omega}\right) \sin \omega t \tag{59}$$

$$v_{C_1}(t) \cong E_b(1 - \cos \omega t) \tag{60}$$

From Eq. (60) it is seen that when

$$t = t_c = \frac{\pi}{\omega} = \pi (L_1C_1)^{1/2}$$

then

$$v_{C_1}(t_c) \cong 2E_b \tag{61}$$

where $t_c \triangleq$ time that capacitor charging current ceases. In practice generally $t_w(\min) > t_c$, where $t_w(\min) \triangleq$ minimum allowable pulse width for conduction of SCR 1.

When the capacitor C1 is charged to a voltage value equal to twice the value of the battery voltage, with respect to ground potential, the battery current flows into the motor circuit according to the following equation:

$$i_a(t) \cong i_a(t_c) \exp\left[-\left(\frac{r_a}{\ell_a}\right)(t - t_c)\right] + \left[\frac{E_b - E_a(t)}{r_a}\right] \times \left\{1 - \exp\left[-\left(\frac{r_a}{\ell_a}\right)(t - t_c)\right]\right\} \qquad t_c \le t \le t_p \tag{62}$$

where

$i_a(t) \triangleq$ instantaneous value of motor armature current

$t_p \triangleq$ period of pulse-width modulator operation

In Eq. (61), the back-emf voltage $E_a(t)$ is assumed to be constant during each cycle of operation. Therefore,

Eq. (61) describes the variation of armature current in a given cycle of operation.

To obtain the second design parameter consider that SCR 1 is turned off by the commutation action of SCR 2. The current through SCR 1 in the reverse direction must at least be equal to the motor armature current. For the worst case, the following equation must be satisfied:

$$C_1 \frac{dv}{dt} = i_a(\max) \tag{63}$$

From Eq. (63),

$$v(t) = E_b + \left[\frac{i_a(\max)}{C_1}\right] t_{off} \tag{64}$$

where t_{off} = turn-off time of SCR 1. If $v(t) \approx 2E_b$ during the turn-off of SCR 1, then

$$C_1 \approx \left[\frac{t_{off}\, i_a(\max)}{E_b}\right] \tag{65}$$

Letting

$$E_b = 24.0 \text{ V}$$

$$t_c = 100.0\ \mu\text{s}$$

$$t_{off} = 12.0\ \mu\text{s}$$

$$i_a(\max) = 10.0 \text{ A}$$

and using Eqs. (61) and (65) yields

$$C_1 = 5.0\ \mu\text{F}$$

$$L_1 = 500.0\ \mu\text{H}$$

A detailed analysis has indicated that a pulse frequency of 250.0 Hz is adequate for the proper variation of the armature voltage.

The following components (Ref. 3) were selected for the design of the step-down voltage converter (Fig. 16):

(1) SCR 1 = C12A (GE); mounted on NC401 heat-sink (Wakefield).

(2) SCR 2 = C9A (GE).

(3) D1, D2 = 1N3881R (GE).

(4) D3 = 1N3882R (GE); mounted on NC301 heat-sinks (Wakefield).

(5) D4 = 1N3883R (GE).

(6) C1 = 28F952 (GE).

(7) CF = 1.0 μF 200.0 V.

(8) L1 = 500.0 μH.

The selection of SCR 1 and SCR 2 is made on the basis of the following considerations:

(1) Turn-off times that are less than, and equal to, 12.0 μs.

(2) Acceptable di/dt and dv/dt capabilities.

b. Design parameters for step-up converter. The design parameters of the SCR dc to dc step-up voltage converter are obtained as described in the subsequent paragraphs.

When SCR 3 is turned on, the values of R1 and C2 are chosen such that $R_1C_2 = 0.25$ ms, since $C_2 = 5\ \mu$F and $R_1 = 50\ \Omega$.

The turns ratio of the step-up transformer is chosen to be 10.0. Resistor R2 is put in series with free-wheeling diode D5, and prevents the saturation of the core of the step-up transformer. Resistor R2 is chosen to be 100 K Ω. Resistor R3 is used for the protection of battery terminals during the regenerative braking action. The value is chosen to be 100.0 Ω. The use of resistor R3 slightly lowers the efficiency of the regenerative braking action at the expense of the protection of battery terminals to large charging currents.

The following components were selected for the design of the step-up voltage converter:

(1) SCR 3 = C12A(GE); mounted on NC301 heat-sink (Wakefield).

(2) SCR 4 = C9A(GE).

(3) D4, D6 = 1N3881R(GE).

(4) D5 = 1N3883R(GE); mounted on NC301 heat-sink (Wakefield).

(5) C2 = 28F952(GE).

SCR 3 and SCR 4 are selected by the same considerations as given for SCR 1 and SCR 2.

C. Laboratory Test Results

The control circuits designed and built according to the concepts described herein have been tested under simulated laboratory conditions. It has been observed that the requirements imposed upon each subsystem are satisfied. A brief summary of important test results follows.

1. *Test results on the pulse-width modulator.* The salient features of the pulse-width modulator are studied by using a high speed oscilloscope fitted with a camera. It has been determined that the pulse-width modulator is capable of varying the conduction duration of main SCRs from 10 to 90% of their maximum conduction durations in the motoring and generating modes of operation.

Figure 17 shows a typical sample of the operational characteristics of the pulse-width modulator for 20 and 80% conduction durations of the main SCR. The negative values of the voltage pulses are caused by the free-wheeling action of the zener diodes placed in parallel with the secondary windings of pulse transformers. The relationship between the input voltage to the base circuit of T39 (see Fig. 12) and the conduction duration of the main SCR is shown to be approximately linear over the workable range.

2. *Test results on the SCR dc to dc step-down and step-up voltage converters.* The voltage waveforms observed across the elements of the SCR dc to dc step-down voltage converter are shown in Figs. 18 and 19 for the 30 and 80% conduction durations of SCR 1, respectively. Similar waveforms were also observed across the elements of the SCR dc to dc step-up voltage converter; for the sake of brevity these are not shown. Figure 20 shows the battery charging voltage across R3 for 20 and 70% conduction durations of SCR 3 observed at a pulse frequency of 225 Hz.

3. *Test results on the minimum-energy controller.* Laboratory tests, carried out for the observation of the combined operation of control circuits described, have shown that the minimum-energy controller controls the vehicle speed in accordance with the theoretical concepts established. This was easily accomplished by applying a desired speed signal, in the form of a step voltage by means of throttle mechanism, into the optimal controller and observing the response characteristics of firing and commutating pulses during the acceleration or deceleration control actions. It has also been shown that the minimum-energy controller has the ability to accelerate, or decelerate, the vehicle from one speed level to any other speed level and to maintain a constant vehicle speed under the variations in the external load, within the allowable speed range.

The prototype development model is shown in Fig. 21. The effect of rolling friction on the dynamical behavior of the system is simulated by using a flexible coupling between the shafts of the drive and load motors.

V. Conclusions

This investigation has demonstrated the application of theoretical concepts of modern control theory in the design of a class of automatic control systems. The minimum-energy controller that is developed is applicable to fractional as well as integral horse-power electric drive systems, providing the components in the dc to dc SCR step-up and step-down converters are selected accordingly and minor adjustments are made in the gain parameters of the system.

The following areas of investigation are left for future work:

(1) The comparison of the energy consumption of the minimum-energy controller with that of the best available commercial speed controller under identical laboratory conditions.

(2) The generation of computer programs to yield all the necessary design information for a particular system of interest.

(3) The replacement of SCRs by power transistors for the low power electric drive systems. This, in turn, drastically reduces the number of components used in the control circuits of the minimum-energy controller.

(4) The determination of a possible application of the minimum-energy controller to electric drive systems using permanent-magnet, brushless dc motors.

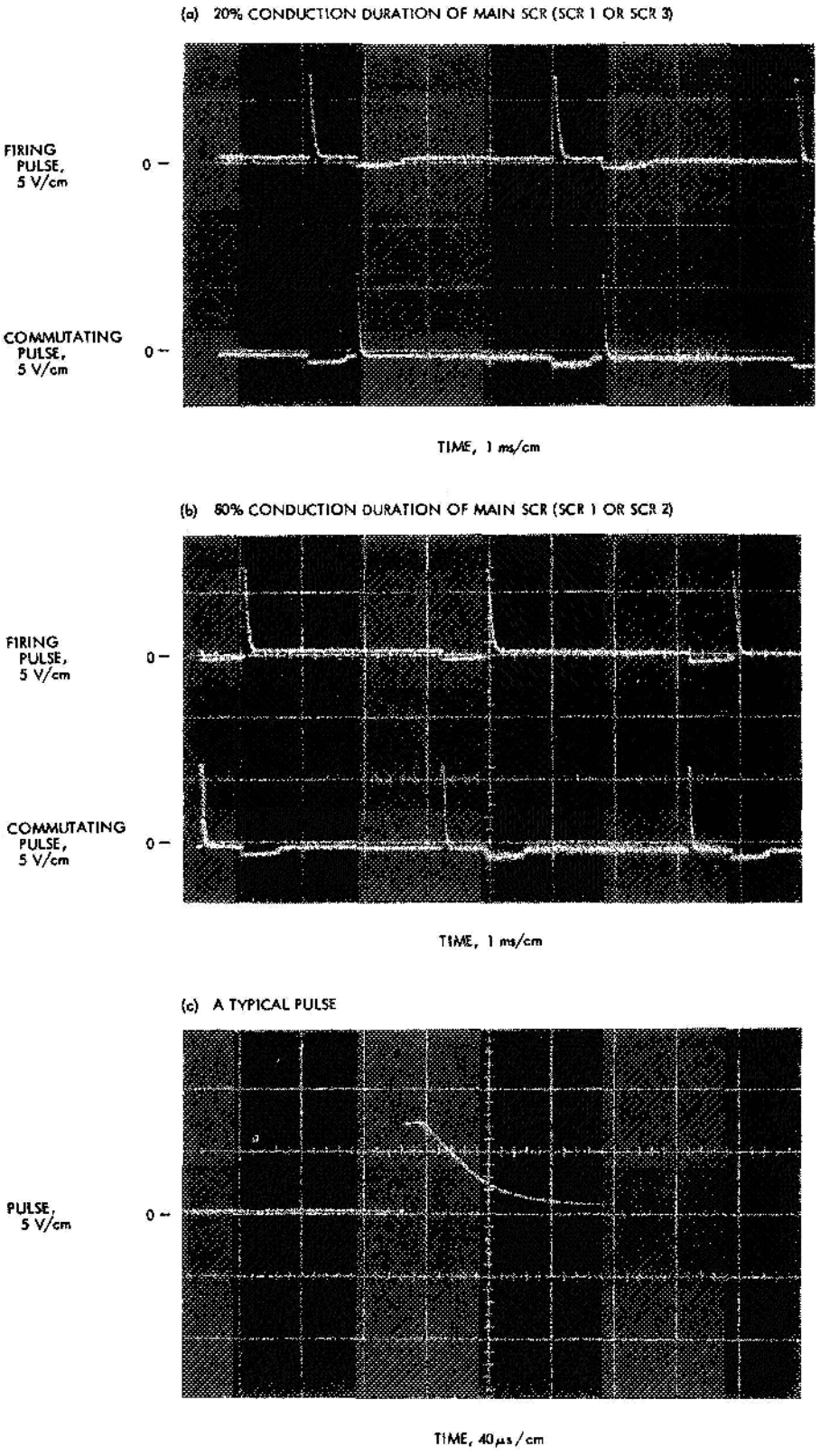

Fig. 17. Operational characteristics of the pulse-width modulator

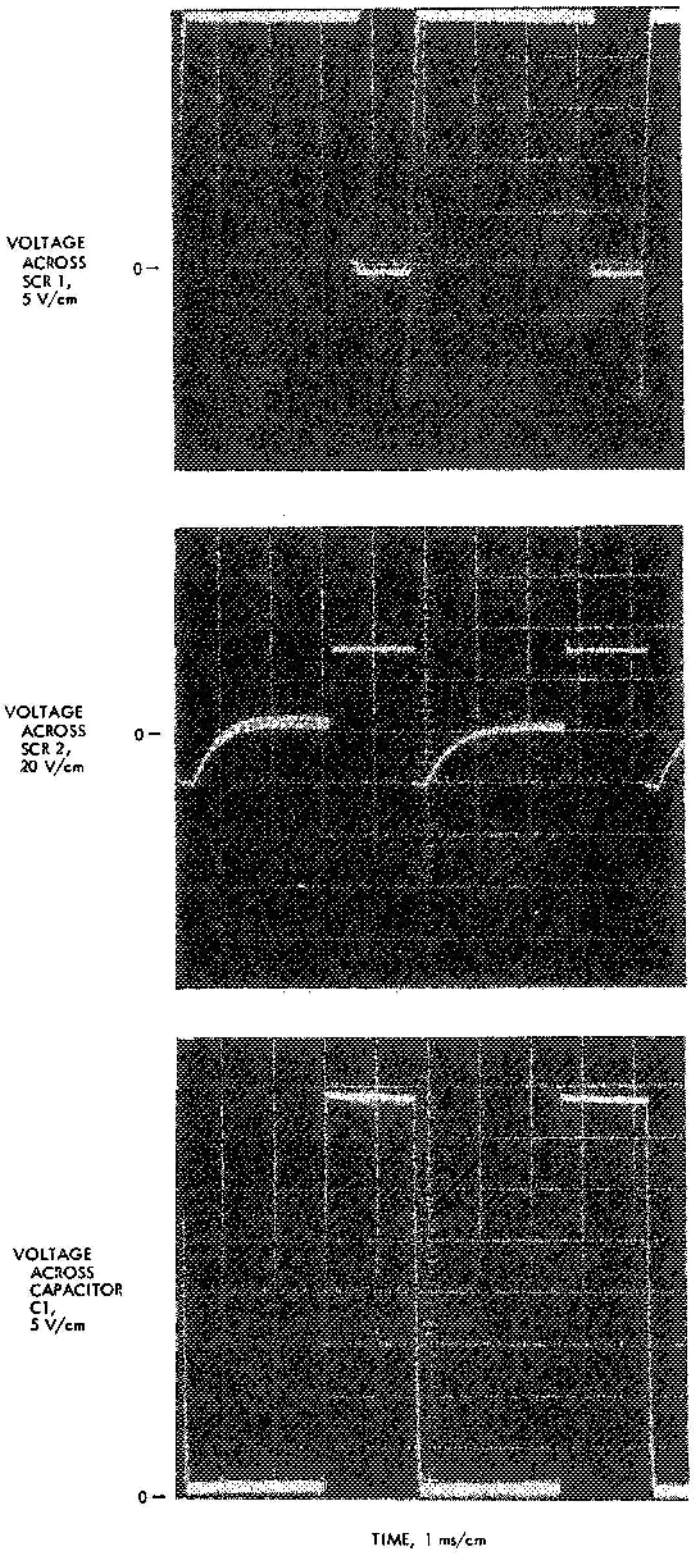

Fig. 18. Operational characteristics of the SCR dc to dc step-down voltage converter for 30% conduction duration of SCR 1

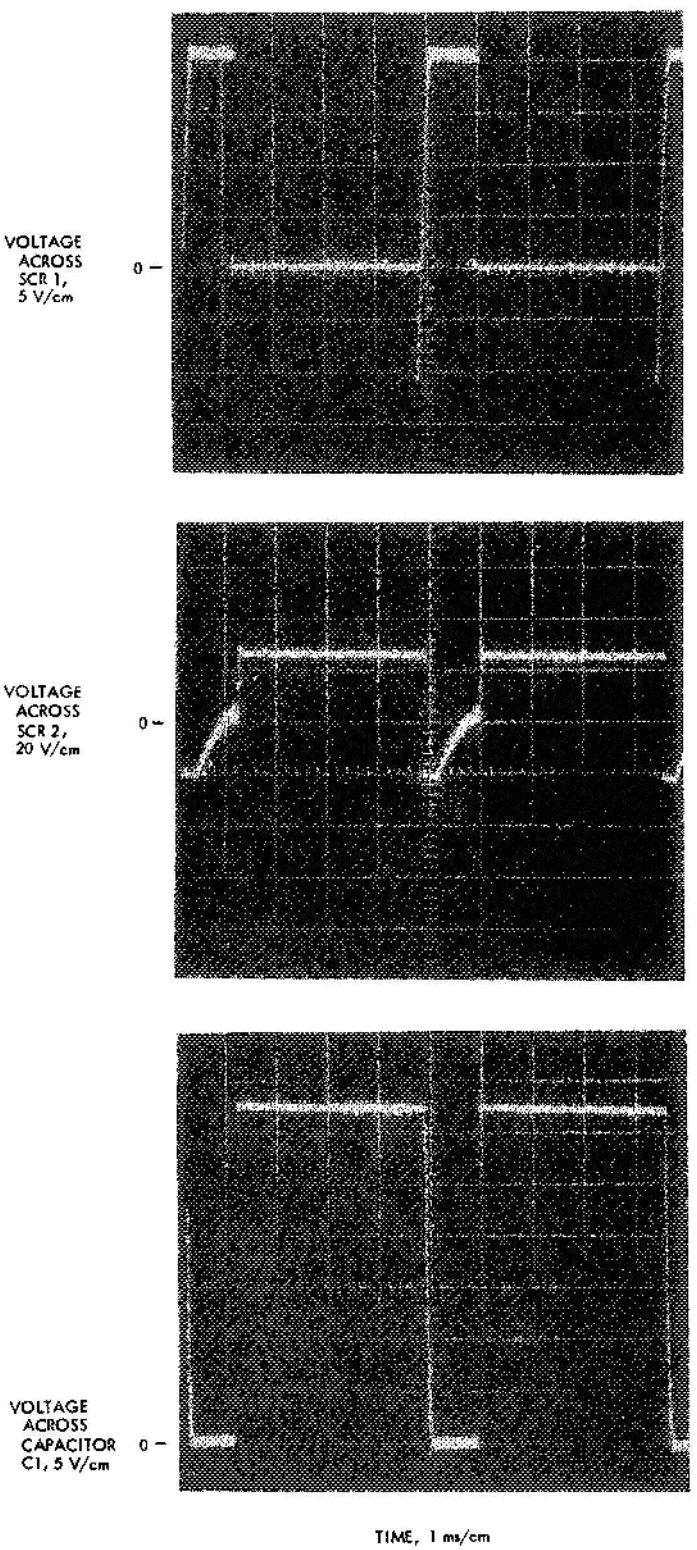

Fig. 19. Operational characteristics of the SCR dc to dc step-down voltage converter for 80% conduction duration of SCR 1

(a) 20% CONDUCTION DURATION OF SCR 3

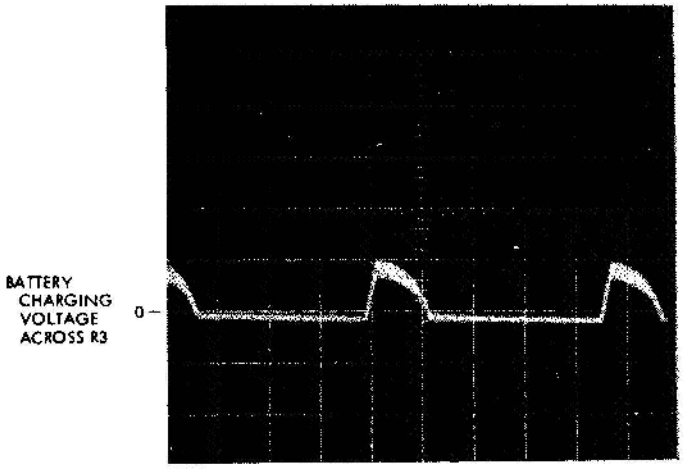

TIME, 1 ms/cm

(b) 70% CONDUCTION DURATION OF SCR 3

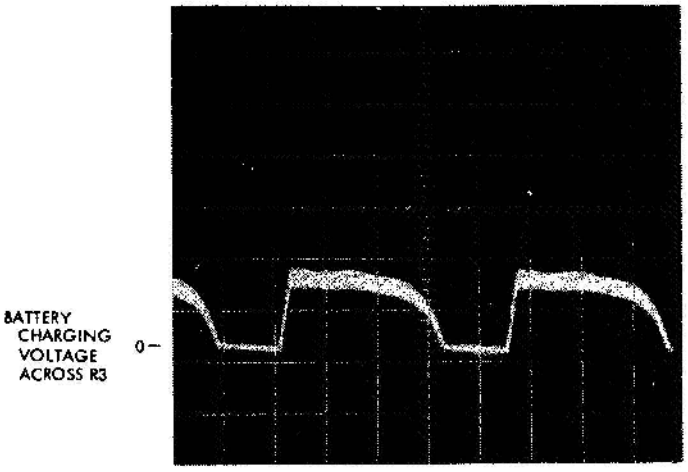

TIME, 1 ms/cm

Fig. 20. Regenerative braking control action

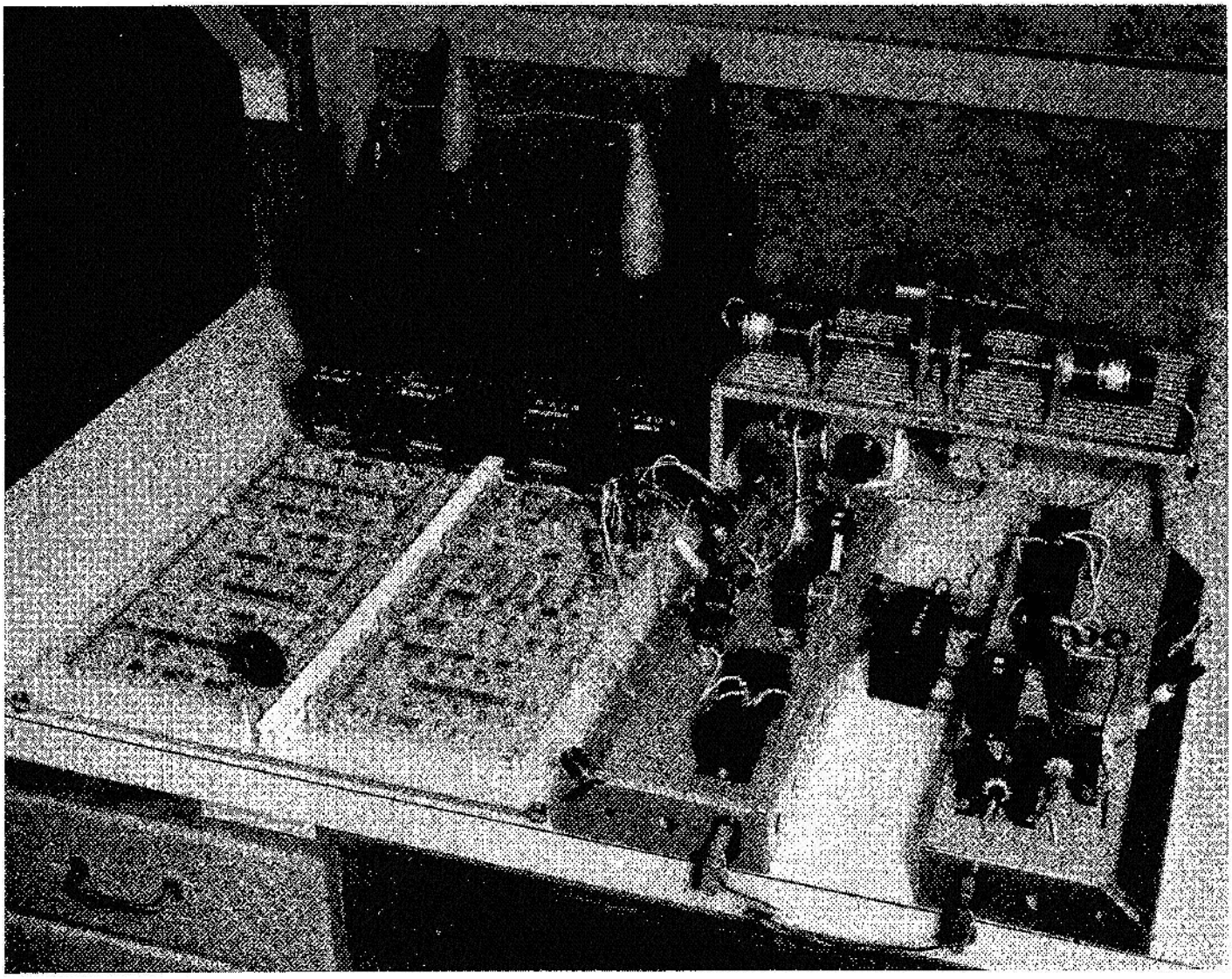

Fig. 21. Prototype development model

Nomenclature

a $\left(\frac{f}{J} + \frac{k_t k_b}{2Jr}\right)$, $a > 0$

b $\left(\frac{k_t^2}{2J^2 r}\right)$, $b > 0$

c $\left(\frac{k_b^2}{2r}\right)$, $c > 0$

C_F conversion factor from ft-lb to Nm

d $a^2 - bc$

$E_a(t)$ back-emf voltage in motor armature

E_b dc supply voltage

F_w weighting factor

f total system damping coefficient as referred to motor, Nm/rad/s

f_1 tire resistance at zero speed, lb

$h(t)$ scalar function

$i_a(t)$ instantaneous value of motor armature current

$i_{C_1}(t)$ instantaneous value of charging current of capacitor C1

J total system inertia as referred to motor, Nm/rad/s

k_b motor back-emf constant, V/rad/s

k_G gear ratio

k_t motor torque constant, Nm/A

ℓ_a constant inductance

$\mathbf{P}(t)$ 3×3 matrix

$\mathbf{Q}(t)$ 2×2 matrix

$\mathbf{q}(t)$ raw vector with three components

$\mathrm{R}(t)$ control variance

r motor resistance

r_a constant dc resistance

r_c dc resistance of diode D1; assumed to be constant

r_w effective radius of wheel-tire assembly, ft

T response time; fixed but arbitrary

t_p period of pulse-width modulator operation

$t_w(\min)$ minimum allowable pulse width for conduction of SCR 1

U battery voltage, V

$u(t)$ control voltage, V

$V_{C_1}(t)$ instantaneous value of voltage across capacitor C1

w_v total weight of vehicle, lb

$x(t)$ angular speed of electric motor; linearly proportional to speed of vehicle, rad/s

$\mathbf{x}$ state vector

$\tilde{x}(t)$ speed dispersion

$x_2(t)$ a stationary Gaussian, exponentially correlated-noise process having zero mean, variance σ_c^2 and correlation time $(1/\omega_0)$, Nm

$x_3(t)$ a constant but arbitrary disturbance torque, Nm

α desired speed of the electric motor, rad/s

$\epsilon[\cdot]$ expectation operator

$\xi_w(t)$ a stationary Gaussian, white-noise process having zero mean and spectral density $2\omega_0 \sigma_c^2$, Nm/s

σ_c standard deviation

$\phi(t)$ slope angle of terrain with respect to local horizontal, deg

ω $\left[\left(\frac{1}{L_1 C_1} - \frac{r_c^2}{4L_1^2}\right)\right]^{1/2}$

ω_0 inverse of correlation time

$<,>$ inner product of two vectors

References

1. Sahinkaya, Y. E., *Minimum Energy Control of Electric Propulsion Vehicles*, Ph.D. Thesis, Electrical Engineering, California Institute of Technology, Pasadena, Calif., Dec. 12, 1968.

2. *Transistor Manual,* Seventh Edition, Unijunction Circuits, General Electric Co., Syracuse, N.Y., 1964.

3. *SCR Manual,* Third Edition, General Electric Co., Auburn, N.Y., 1966.

NASA — JPL — Coml., L.A., Calif.